# THE PERFORMANCE
# OF
# HORIZONTAL-CRESTED LINEAR PIPE EXPANSIONS
# AS
# SERVICE RESERVOIR INLETS

by

David Alan Smith

Submitted in partial fulfilment of the
requirements for the degree of
Master of Applied Science

Department of Civil Engineering
School of Graduate Studies
University of Ottawa
Ottawa, Canada

June 1976

# PREFACE

This thesis presents the findings of a laboratory investigation of the performance of horizontal-crested linear expansions as inlet structures for covered service reservoirs.

The main advantages to using this type of inlet structure is the opportunity to thoroughly aerate the water, by the fountain-like action of the expansion, and the independence of the pressure in the supply main on the varying water surface level in the reservoir, eliminating the need for reflux valves in the supply line and permitting the pumping main to be emptied when the pumps are not operating.

Since the space between the maximum height to which the water rises and a point just below the crest of the expansion is not available for storage, the designer will wish to know quite accurately how high the fountain will rise. The designer will, however, want to avoid having the turbulent water jet repeatedly striking the roof of the reservoir.

Bellmouth expansions have the same main advantages as simple linear expansions, however they are more expensive to construct and, for a given discharge, have a signifigantly higher maximum dome height than the equivalent[1] linear expansion.

A total of 10 expansions were tested. These were four 45.7 cm-long expansions with internal angles of 7, 20, 33 and 45 degrees; four 22.8 cm-long expansions with

---

[1] defined by equating the perimeters at the expansion crest.

the same internal angles as the 45.7 cm expansions; a bellmouth, equivalent to the 33° 45.7 cm expansion, and a straight pipe extension. The inlet diameter of each expansion was 7.82 cm. The maximum discharge investigated was approximately 12 l/s.

A dimensional analysis indicates that to transfer from the laboratory scale investigated to the prototype situation and maintain similarity, the discharge in the prototype should equal the product of the discharge in the model and the ratio of the diameter in the prototype to the diameter in the model raised to the power of 2.5.

The maximum dome heights were measured using a model 157-B Level-Tel transmitter and probe. This is a capacitance sensing system which provided a continuous record of water level when interfaced with a Hewlett Packard strip chart recorder.

It was found that the 33° gave the best performance in reducing the maximum dome height. This height was reduced by at least 50 per cent for this expansion angle by doubling the length from 22.8 cm to 45.7 cm. The 20° expansion performed almost as well as the 33° expansion in dissipating the energy of the jet. Both of these inlet structures, however, displayed rapidly fluctuating dome positions (most apparent for the 22.8 cm expansions).

The rapid fluctuations in dome position could cause severe lateral movement of the expansion and the inlet

pipe; therefore, a method of reducing the severity of these fluctuations and, hence, vibrations and stresses was tested with signifigant success. The technique is to add horizontal slotting running around the circumference of the expansion, just below the crest. These slots occupied 33 per cent of the circumference.

A dye injection study was performed on 4, half-section expansions (internal angles: 7, 20, 33 and 45 degrees). This investigation indicated jet separation from the expansion walls very near the entrance for low discharges. For higher flows, the jet would often move to a wall, especially for the 20 and 33 degree expansions. Little, if no expanding of the width of the jet occured.

## ACKNOWLEDGEMENTS

I wish to express my sincere gratitude and appreciation to my supervisor, Dr. D. R. Townsend, for providing the laboratory facilities and guidance throughout the project. Thanks are due to Mr. Robert Moore and Mr. Gregg Duchesne for constructing the major components of the apparatus. Thanks are also due to Mr. Ron Howatt for drafting the figures.

I must also express my appreciation to the Federal Department of the Environment for granting me educational leave and financial assistance to study at the University of Ottawa.

## TABLE OF CONTENTS

## LIST OF FIGURES

## LIST OF PLATES

## LIST OF TABLES

## NOTATIONS

| | |
|---|---|
| $A(\ell)$ | = Lateral area of momentum jet |
| $b$ | = Width of the rectangular weir |
| $C = Q/bh^{1.5}$ | = Constant for the calibration of the rectangular, sharpcrested weir. |
| $C_1 = Q/Ph^{1.5}$ | = Constant for the calibration of the horizontal-crested expansions |
| $C_2 = C_1P$ | = Constant for the calibration of the horizontal-crested expansions |
| $D$ | = Diameter of the inlet or nozzle |
| $f$ | = Function of |
| $F_n = \overline{V}/\sqrt{gD}$ | = Froude number[1] |
| $g$ | = Gravitational constant |
| $G$ | = Constant |
| $H$ | = A general term to indicate the maximum dome height (see $H_{10}$)[2] |
| $H_{10}$ | = Maximum dome height - the level to which the water rose (or exceeded) for ten per cent of the time |
| $h$ | = Overflow water level for the expansions measured above the crest |
| $h'$ | = Head of water above base of slots in slotted expansions |
| $I$ | = Constant |
| $k$ | = Roughness value for expansion walls |
| $L$ | = Length of expansion |
| $\ell$ | = Jet width |
| $M$ | = Momentum flux along jet trajectory |

[1] Sellin(1) uses $F_n = \dfrac{\overline{V}^2}{gD}$ (see Figures 6 and 7)

[2] Sellin(1) uses H as $H_{10}$ (see Figures 6 and 7)

$M_o$ = Momentum flux from source

$m = M/\rho$ = Kinematic momentum flux

$m_o$ = Kinematic momentum flux at source

$n_x$ = Ratio of the magnitude of parameter x in the prototype to parameter x in the model

P = Perimeter of the crest of the expansion

q = Volume flux along jet trajectory

Q = Flow through the expansion (includes flow through slots of slotted expansions

$q_o$ = Volume flux at source of momentum jet

$Q_e$ = Flow in the half-section expansions multiplied by two

$Q_s$ = Discharge through the slots of the slotted expansions

$R_e = \frac{\rho \bar{V} D}{\mu}$ = Reynolds number

r = Radial coordinate from the jet centerline

s = Coordinate along the jet centerline from the source

t = Time

$u_L = \frac{m}{q}$ = Mean velocity characterizing mass flux along the jet path

u(r) = Local jet velocity parallel to the jet axis at a point a distance, r, from the axis

$u_m$ = Maximum value of u(r), which occurs at the centerline

$u_o$ = Initial velocity of jet at source

$\bar{V}$ = Mean velocity of flow at entrance to expansion

w = Radial entrainment velocity occurring at $r = \ell$

| | |
|---|---|
| $\alpha'$ | = An entrainment coefficient |
| $\beta$ | = An entrainment coefficient |
| $\sigma$ | = Standard deviation of the velocity distribution |
| $\rho$ | = Density of water |
| $\phi$ | = Function of..... |
| $\eta = \frac{r}{l}$ | = Ratio of the radial coordinate from the jet centerline to the jet width |
| $\mu$ | = Dynamic viscosity of water |
| $\alpha$ | = Internal angle of expansion |
| $K_n$ | = A constant (n = 1,2,3,4) |

# CHAPTER 1

# INTRODUCTION

## 1.1 Service Reservoirs

Service reservoirs are used to store water. Often they also serve as balancing reservoirs to maintain adequate pressure throughout a water distribution system. The storage capacity of a service reservoir is dictated by the maximum volume of water required to meet the demands on the system. This quantity of water is calculated from an estimate, or knowledge, of the variation of demand with time and the average demand.

Service reservoirs may be covered or uncovered. The covered reservoir, the preferred alternative today, prevents contamination of the supply by debris and birds; reduces the risk of freezing and excessive heating in the reservoir; prevents the growth of algae which is promoted by sunlight; practically eliminates evaporation losses; and prevents the accidental loss of life by drowning.

## 1.2 Service Reservoir Inlets

A service reservoir that is being used to balance pressure in a large distribution system normally has a common inlet/outlet structure which must be located below the waterline, normally in the floor or a wall of the reservoir. A service reservoir, functioning principally for storage and requiring only local distribution of supply or having a locally available source of water, can be equipped with separate inlet

and outlet structures. Generally speaking, there are two configurations for inlets to service reservoirs of this type. These are the horizontal supply, which has a submerged jet, and the vertical supply with a free surface (see sketch below).

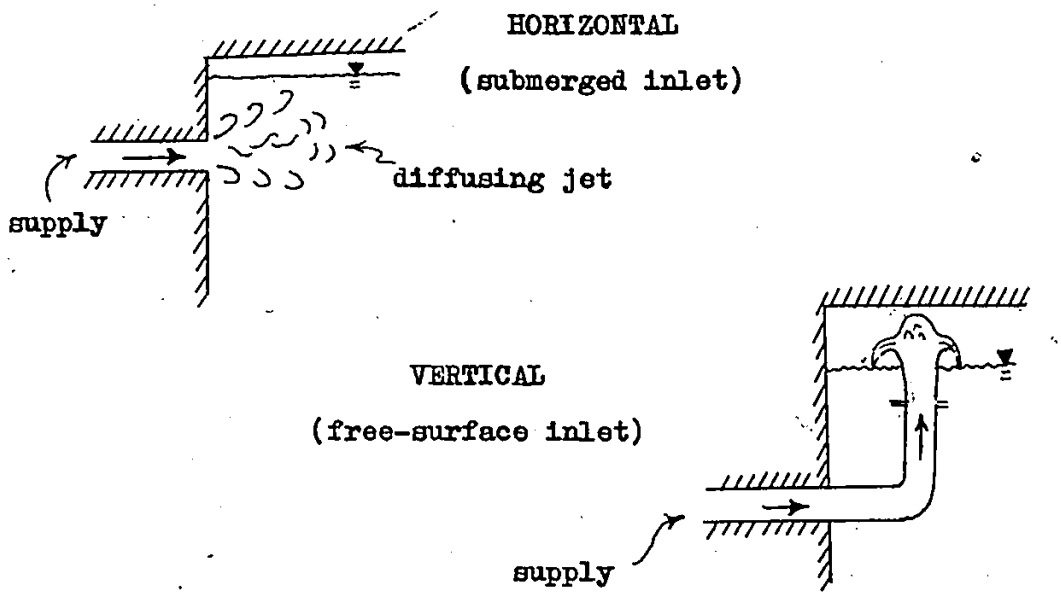


The submerged inlet has two signifigant consequences. First, if the water supplied to the reservoir has a low oxygen content (often the case if the source of supply is groundwater), there is little opportunity to aerate the supply, other than through the relatively calm water/air interface. Second, the supply main pressure is dependent on the varying water surface level within the reservoir. This latter point applies to service reservoirs that are dependent on a pumped supply from a lower level. In this case an increase in the water surface level in the reservoir could cause a back-up of water in the supply main, therefore reflux valves must be supplied to prevent this.

The vertical supply, on the other hand, allows the water supplied to the reservoir to be aerated (an advantage to the use of this type of structure in water/wastewater treatment) and causes the pressure in the supply main to be independent of the varying water surface level. Since no back-up of water is expected, reflux valves are not needed. The supply main can also be drained when the pumps are not operating. This prevents freezing of the supply line.

In order to determine how far from the roof of the reservoir to locate the crest of the vertical supply inlet, some knowledge of the height to which the water will rise above the crest of the inlet for any particular discharge is required. The inlet structure must be positioned to avoid the possibility of strong vibrations being set up in the roof of the structure by repeated impact of a turbulent water jet. If the frequency of the blows approached the resonant frequency of the structure, these vibrations could be quite dangerous.

## 1.3 Linear Expansion Inlet Structures

Bellmouth expansions have been used as expansion overflow structures (1), however it seems that simple linear expansions (see sketch on the following page) should perform just as well in this context. Obviously a simple linear expansion would be a cheaper alternative.

In addition to the savings due to the simple linear shape, linear expansions should produce a lower maximum dome height than a bellmouth with the equivalent diameter at the crest. This lower maximum dome height will permit the linear

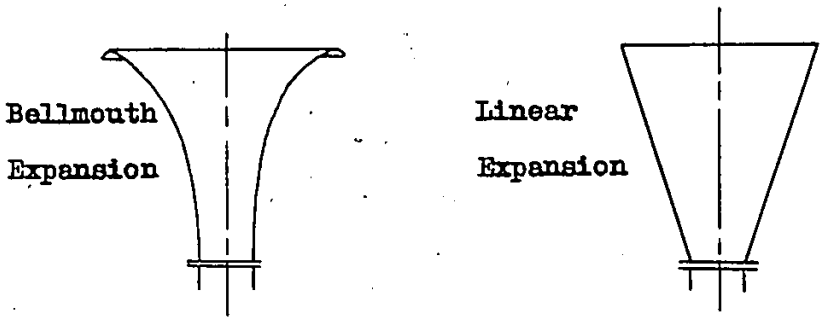


expansion to be located closer to the roof of the reservoir than the equivalent bellmouth, thereby permitting a greater volume of water to be stored in a given service reservoir.

The maximum dome height for the bellmouth expansion at a particular discharge is greater than that for the linear expansion (see Fig. 1). This is due to the small change in width of the bellmouth expansion with distance from the base of the inlet structure. The confined environment in the bellmouth expansion does not permit as much turbulent mixing to occur between the rising jet and the expansion walls, resulting in much higher jet velocities near the crest of the expansion, and hence the greater rise of the water above the crest.

In Fig. 1, on page 5, the dome indicated by a dashed line is that for the bellmouth expansion. The dome drawn as a solid line is that for the equivalent linear expansion. The $\Delta H$ is therefore the difference between the maximum dome heights for the bellmouth and the linear expansion at a given discharge.

COMPARISON OF PERFORMANCE OF LINEAR EXPANSION AND EQUIVALENT BELLMOUTH

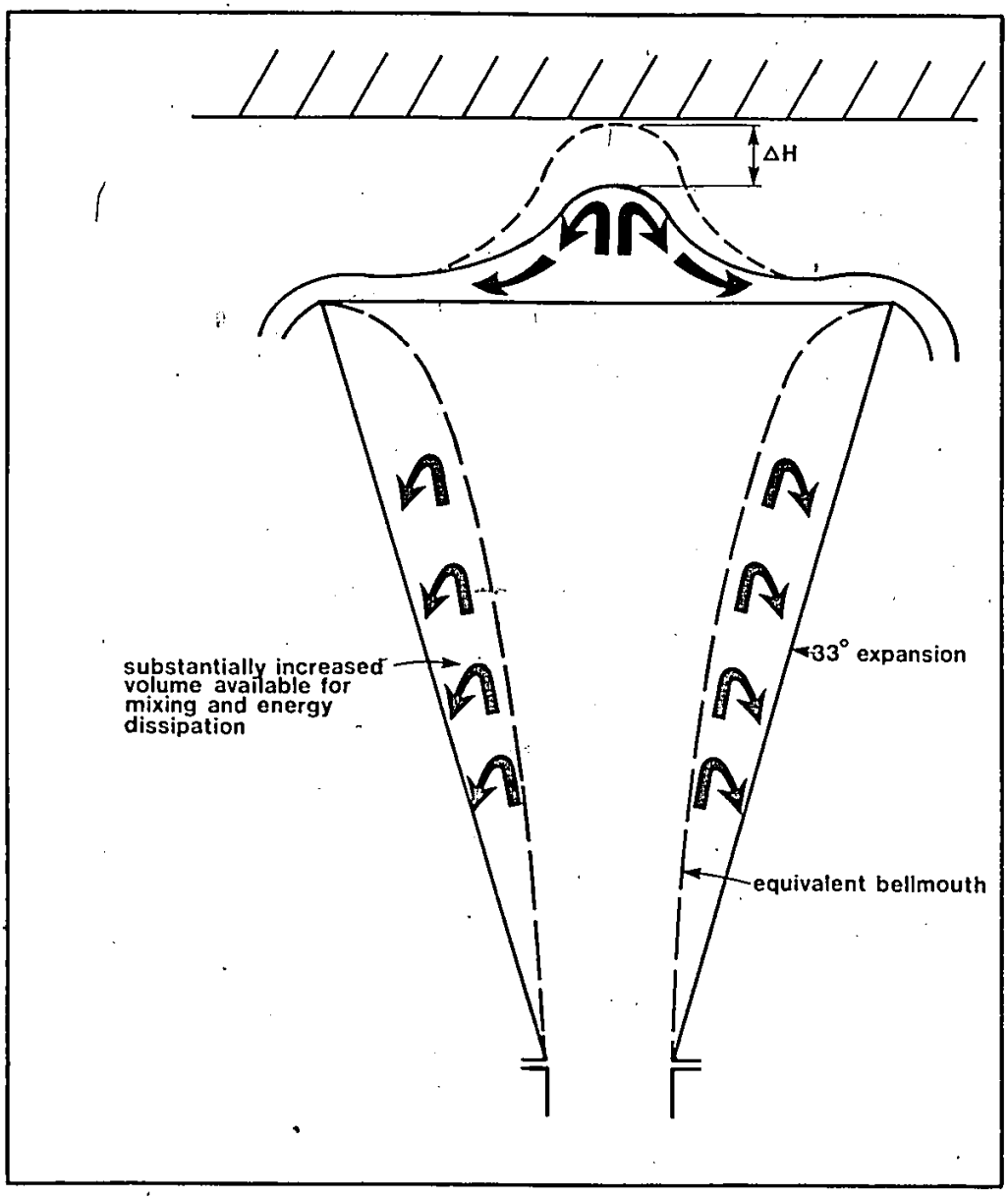


Figure 1

## 1.4 Laboratory Program

The laboratory program described in this thesis was undertaken to test the suitability and performance of horizontal-crested, linear pipe expansions as service reservoir inlets. Four expansion angles were investigated (7, 20, 33 and 45 degrees). It was considered to be unlikely that an expansion with an internal angle much less than 7 degrees would produce dome heights signifigantly different than a straight pipe section. It was also considered that an expansion with an internal angle greater than 45 degrees would provide more than enough volume and width for the expansion of a momentum jet, and that any greater angle would result in an increase in dome height for a particular discharge due to the entrainment of water located between the edge of the jet and the walls of the expansion.

A schematic diagram of a linear expansion, along with an explanation of the notation used in this study, is given in Fig. 2.

To provide a basis for comparison, a straight pipe extension section and a bellmouth expansion (with a perimeter at the crest equal to that of the 33 degree linear expansion) were also tested. Scale diagrams of the various expansions' internal dimensions and the straight pipe unit are presented in Figure 3.

## LINEAR EXPANSION NOTATION

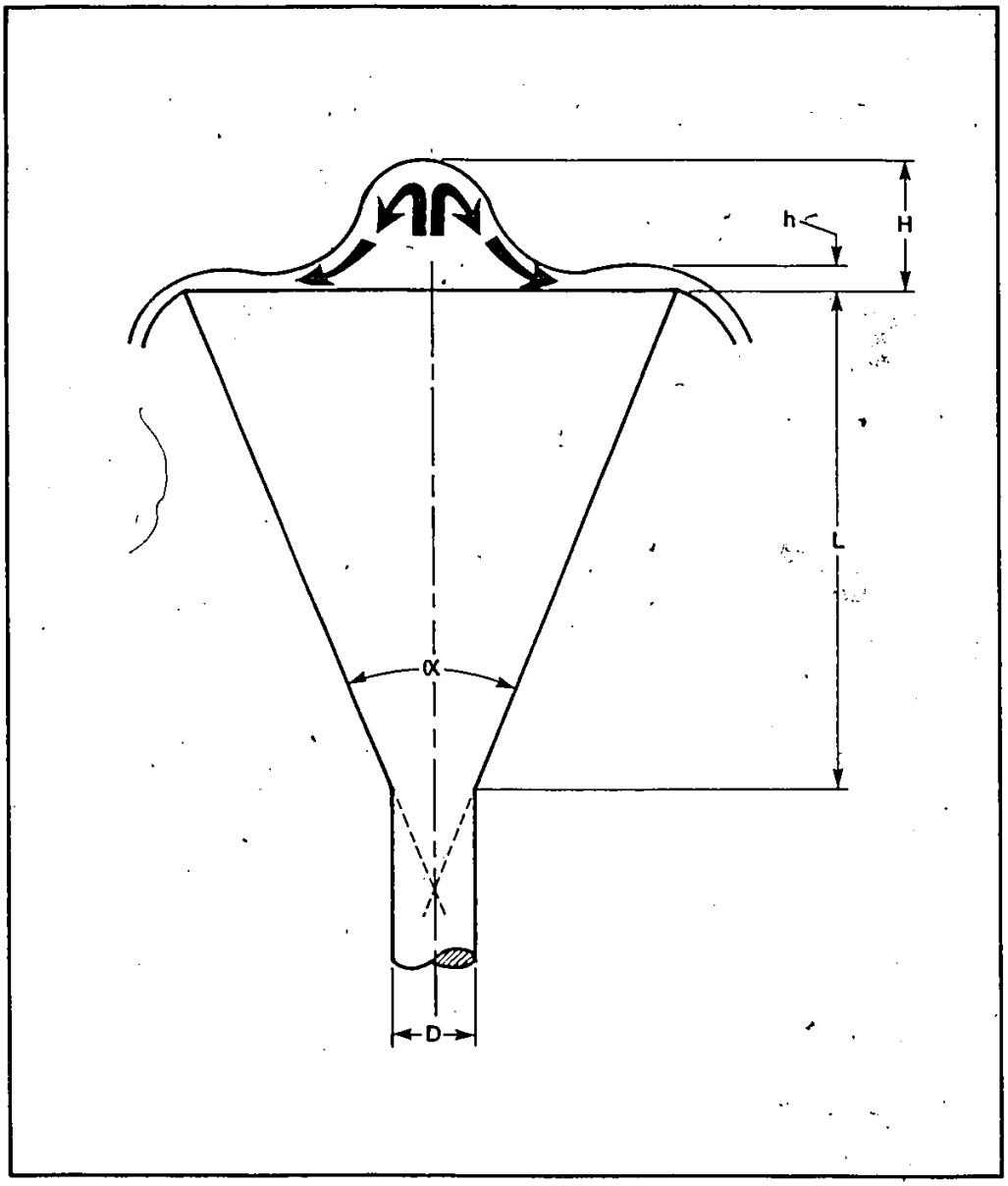


Figure 2

## EXPANSION INTERNAL DIMENSIONS AND SHAPES

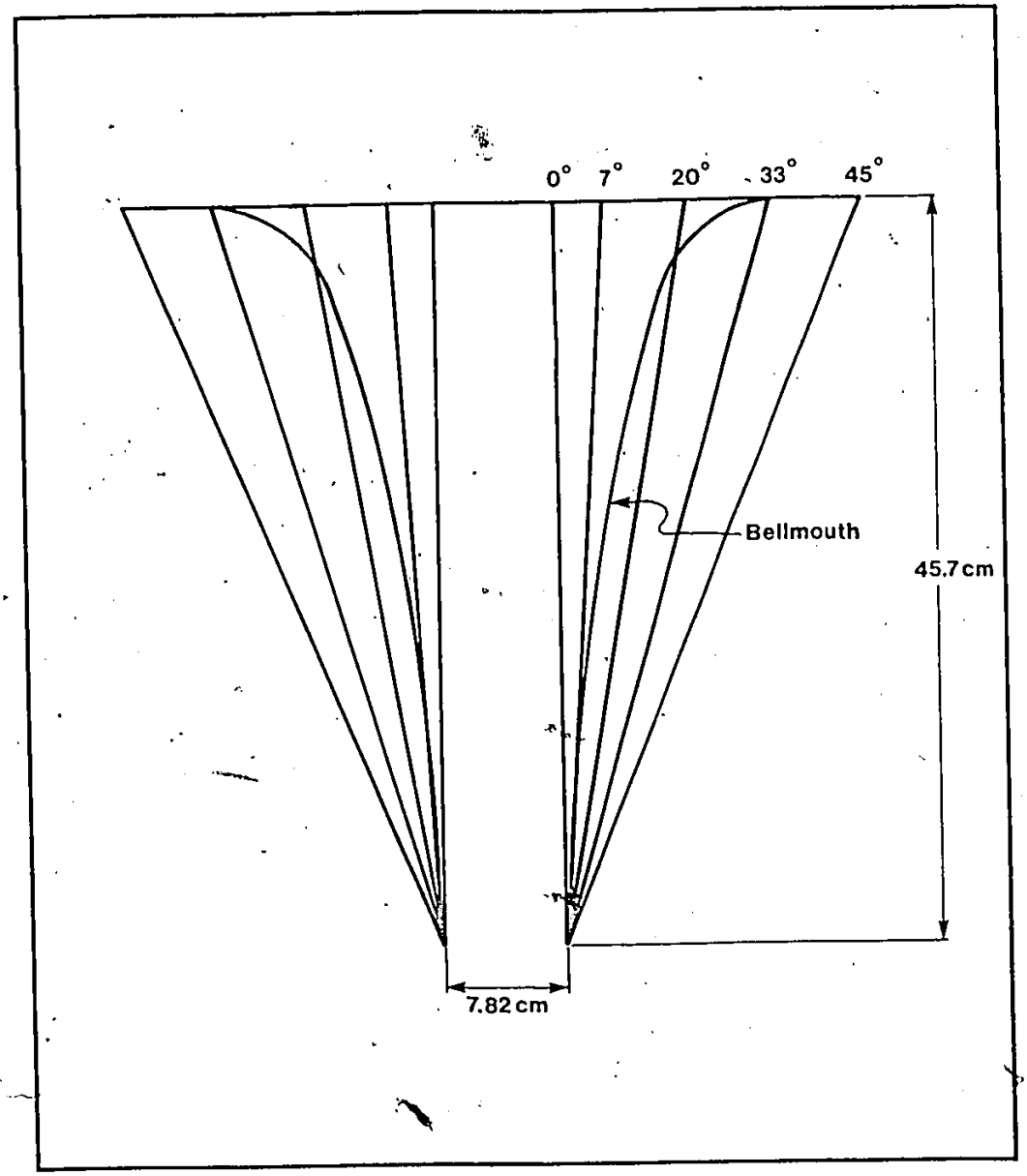


Figure 3

# CHAPTER 2

# THEORETICAL CONSIDERATIONS AND LITERATURE REVIEW

## 2.1 Jets

### 2.1.1 General Remarks

The successful design of outfall diffusers for both sewage disposal and the discharge of cooling water from thermal power plants necessitates mathematical solutions for a wide selection of jet and plume diffusion problems. The simplest case of jet diffusion is a pure momentum jet, in which the jet and the ambient fluid have identical density. Cederwall (2) has recently presented gross parameter solutions for a variety of flow situations for jets and plumes. One of these is the simple case referred to above which is the case under investigation in the laboratory investigation of linear pipe expansions.

For the pure momentum jet, with the densities of both the jet and ambient fluid identical, the trajectory is a straight line. When the jet penetrates the ambient fluid, a turbulent mixing layer develops, which diffuses both momentum and mass laterally. Initially it is found that an unstable shear zone, just a few diameters long, adjusts the flow structure to that of a fully developed region (zone of established flow) (2). Lengthwise velocity profiles across the jet are of a similar shape.

Problems of jet diffusion have received a great deal

of attention in the past. A number of investigators have adopted an integral technique when analyzing jet and plume flow situations. In these studies self-similar distributions of velocity and density were assumed and the problem was stated by taking as a control volume a thin slice of the flow field extending laterally across the jet. The rate of change of the bulk characteristics of the jet flow in terms of the axial jet velocity, axial density, and jet width was then described by the equations of conservation of mass and momentum. The velocity and density profiles chosen were often of the Gaussian type and the entrainment velocity at the edge of the jet was assumed to be proportional to the jet velocity at the axis. A comprehensive study of turbulent jet and and plume problems, following this analytical technique has been summarized by Fan and Brooks (3).

Cederwall (2) demonstrated how the integral technique for analyzing turbulent jet and plume problems may be further simplified. Gross parameter solutions for virtual point or line sources were presented for a number of flow situations but limited to stagnant, homogeneous, or linearly density-stratified ambient water. In principle, the solutions include only one empirical constant, relating the rate of entrainment to the gross variables of the flow. Cederwall found that dimensional reasoning could be used to establish effectively the fundamental features of the turbulent flow field generated by jet or plume sources.

### 2.1.2 Analysis of Momentum Jets

A momentum jet is characterized by an initial flux of

momentum - there is no buoyancy flux. The ambient fluid is not necessarily homogeneous; however, this discussion will be restricted to this case since it applies directly to the linear expansions under investigation.

The assumptions underlying the analysis of a momentum jet are:

1. The fluid is incompressible
2. The generated flow field is fully turbulent, which means that Reynolds number dependence is absent.
3. Mass and momentum are assumed to diffuse at the same rate.

A volume source is considered, a real source, of initial mass and momentum flux only. A virtual origin of the jet (mathematical source) may now be defined in such a way that for $s \to 0$:

$$M_o = \rho_o q_o u_o \sim (u_o D)^2 \Rightarrow \text{constant value} \quad \ldots\ldots (1a)$$

$$q_o \sim (u_o D) D \Rightarrow 0 \quad \ldots\ldots\ldots\ldots\ldots\ldots (1b)$$

in which:

s is the distance from source,

$M_o$ is the momentum flux at the source,

$u_o$ is the initial velocity,

D is the diameter of the nozzle, and

$\rho$ is the density of the fluid.

This definition requires that $D \Rightarrow 0$. Thus, this is an idealized point source characterized by an initial momentum flux only.

It has the same dynamic impact on the surrounding quiescent fluid as a corresponding volume source displaced a short distance - approximately one diameter from the nozzle - in the negative flow direction in order to reproduce the mass flux at the point where the volume source is located.

Some basic features of jets follow from dimensional reasoning. Before applying the fundamental principles of fluid mechanics in formulating the governing equations it is useful to demonstrate how dimensional arguments can be used to establish some pertinent information on the behavior of a three-dimensional jet in a uniform density environment. Figure 4 shows a vertical jet that issues from a point source. For the dimensional analysis use is made of the following independent variables describing the flow problem: r, the radial coordinate originating from the jet centerline; s, the coordinate along the jet centerline; g, the acceleration of gravity; $\rho$, the density of the fluid; $M_o$, the momentum flux from source. A kinematic momentum flux from the source, $m_o$[1], is also defined.

The dependent variables are: M, the momentum flux along the jet trajectory; q, the volume flux along the jet trajectory; m, the kinematic momentum flux; u(r), the local jet velocity parallel to the jet axis at a distance, r, from the axis [in which u(r) has its maximum value $u_m$]; $u_m$, the centerline velocity as defined previously; $\ell$, is the typical jet width; and w, the radial entrainment velocity appearing at $r = \ell$. The following

---

[1] the kinematic momentum flux, m, equals the momentum flux, M, divided by the density of the fluid.

AXIAL-SYMMETRIC JET

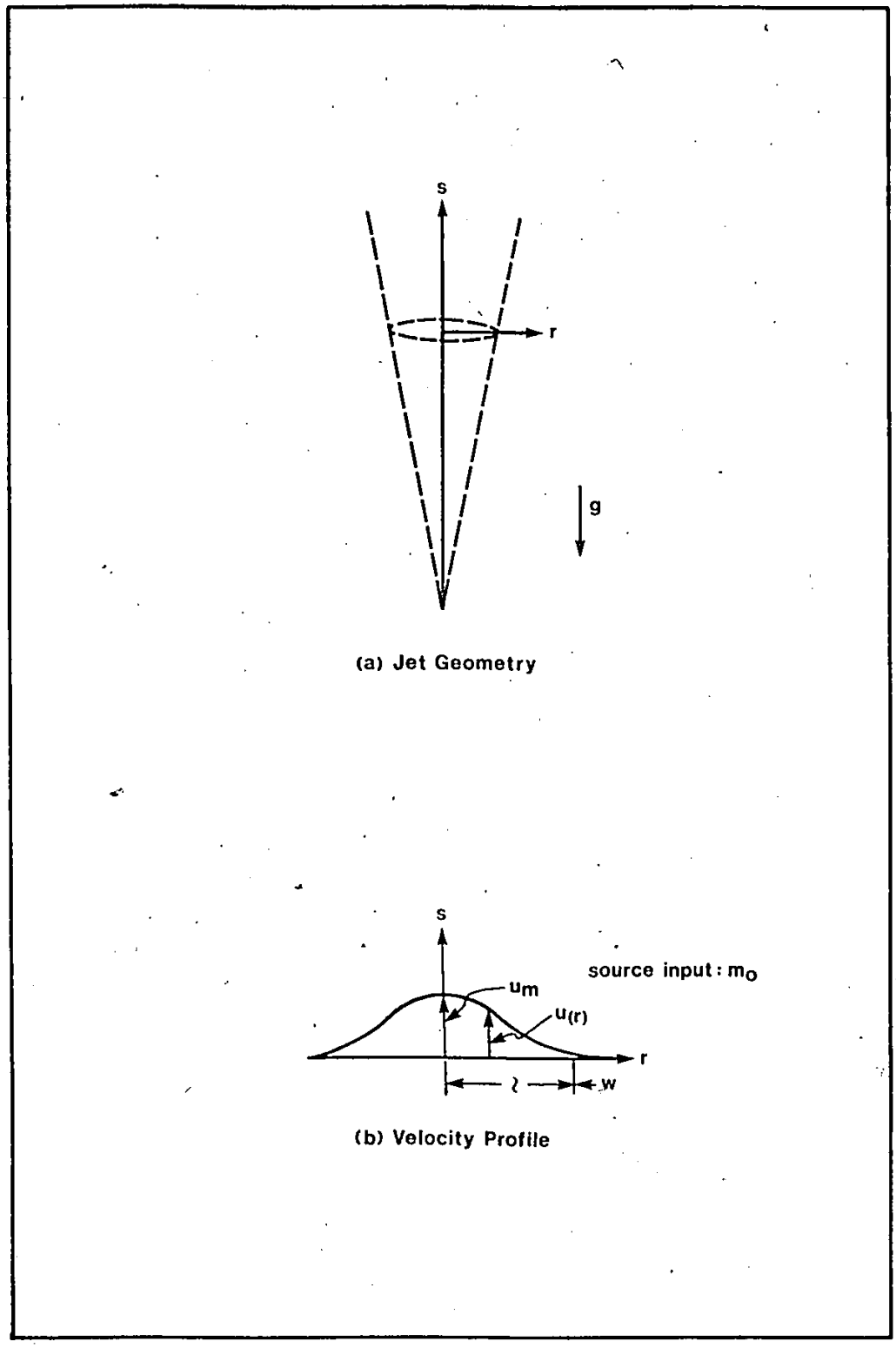


Figure 4

functional relationships follow from dimensional reasoning.

Volume Flux

The flow, q, induced by the source is related to the source input:

$$f\left[m_o, s, q\right] = 0 \quad \ldots\ldots\ldots\ldots\ldots\ldots \quad (2)$$

Thus, the flow is expressed by a dimensionless parametric grouping:

$$\frac{q}{s m_o^{1/2}} = K_1{}^{1} \quad \ldots\ldots\ldots\ldots\ldots\ldots \quad (3)$$

Lateral Velocity Distributions

Dimensional analysis implies that the following relations must hold for the typical jet width, $\ell$, and the velocity profile, u(r):

$$\frac{\ell}{s} = K_2{}^{1} \quad \ldots\ldots\ldots\ldots\ldots\ldots \quad (4)$$

$$\frac{u(r)s}{m_o^{1/2}} = f\left(\frac{r}{cs}\right) \quad \ldots\ldots\ldots\ldots\ldots\ldots \quad (5)$$

Similarly, for the momentum flux:

$$\frac{m}{m_o} = K_3{}^{1} \quad \ldots\ldots\ldots\ldots\ldots\ldots \quad (6)$$

Eq. 3 can be rewritten to relate to a real source:

$$\frac{qD}{q_o s} = K_4{}^{1} \quad \ldots\ldots\ldots\ldots\ldots\ldots \quad (7)$$

Also, Eq. 5 can be written:

---

[1] $K_n$ are constants

$$\frac{u(r)s}{u_o D} = f\left(\frac{r}{s}\right) \quad \ldots\ldots\ldots\ldots\ldots\ldots (8)$$

and consequently:

$$\frac{u_m s}{u_o D} = K_5 \quad \ldots\ldots\ldots\ldots\ldots\ldots (9)$$

Combining Eqs. 8 and 9:

$$\frac{u(r)}{u_m} = f\left(\frac{r}{s}\right) \quad \ldots\ldots\ldots\ldots\ldots\ldots (10)$$

and using Eq. 4, Eq. 10 is modified to:

$$\frac{u(r)}{u_m} = f\left(\frac{r}{l}\right) \quad \ldots\ldots\ldots\ldots\ldots\ldots (11)$$

Eq. 11 proves the validity of the principle of similarity for the lateral velocity profile.

We can write for the velocity profile within the jet:

$$u = u_m f(\eta), \text{ where } \eta = \frac{r}{l} \quad \ldots\ldots\ldots (12)$$

The following relationships then hold for the volume flux, q, and the momentum flux, m:

$$q = 2\pi u_m l^2 \int_0^\infty \eta f(\eta) d\eta = 2\pi u_m l^2 I \quad \ldots\ldots (13)$$

$$m = 2\pi u_m^2 l^2 \int_0^\infty \eta f(\eta) d\eta = 2\pi u_m^2 l^2 G \quad \ldots\ldots (14)$$

in which I and G are constants.

One of the main difficulties when analyzing turbulent jet phenomena is specifying the rate of growth of the jet. Cederwall (2) found that the entrainment velocity, w, appearing at the edge of the jet is proportional to the center line velocity, $u_m$, or, as self-similarity of the

velocity profile was shown, the rate of entrainment can be related to the gross properties of the flow:

$$w \backsim \frac{m}{q} \quad \ldots\ldots\ldots\ldots\ldots\ldots \quad (15)$$

The constant of proportionality, an entrainment coefficient, is an empirical coefficient that must be determined experimentally.

Cederwall (2) found from dimensional arguments that for jets, plumes and buoyant jets produced by virtual sources of no initial mass flux, the entrainment coefficient is a constant. The claim that the coefficient of entrainment is a constant for a mathematical source evidently does not hold for volume sources (4). However, from an engineering point of view, it is normally justified to use a constant value for this coefficient.

Momentum Flux

The momentum flux, m, and the volume flux, q, are Eulerian quantities; however, they will be included in the following Lagrangian equations for a three-dimensional situation (a three-dimensional jet in a homogeneous environment).

$$\frac{dm}{dt} = 0 \quad \ldots\ldots\ldots\ldots\ldots\ldots \quad (16)$$

in which t is a time variable defined by:

$$\frac{ds}{dt} = u_L \quad \ldots\ldots\ldots\ldots\ldots\ldots \quad (17)$$

and $u_L$ is then a Lagrangian velocity. Therefore, a control

volume has been assumed that is moving along the jet path with a velocity, $u_L$, so that there is no net momentum flux passing through the control volume. Consequently:

$$\int_{A(\ell)} \rho u(u - u_L) dA(\ell) = 0 \quad \ldots\ldots\ldots\ldots \quad (18)$$

in which $A(\ell)$ is the lateral area of the moving control volume and is a function of the typical jet width only.

Eq. 18 can be written:

$$m - u_L q = 0 \quad \ldots\ldots\ldots\ldots\ldots\ldots \quad (19a)$$

$$\text{or, } u_L = \frac{m}{q} \quad \ldots\ldots\ldots\ldots\ldots\ldots \quad (19b)$$

Eq. 19b defines a mean velocity that characterizes mass flux along the jet path. The only change in momentum is then within the moving control volume expressed by equation 16.

Conservation of Volume Flux

Since the fluids are assumed to be incompressible, the equation for conservation of mass flux turns into a similar relation for the continuity of volume flux.

For a three-dimensional source, the entrainment coefficient, $\beta$, is defined as:

$$\frac{dq}{ds} = \beta s \frac{m}{q} \quad \ldots\ldots\ldots\ldots\ldots\ldots \quad (20)$$

The preceding dimensional analysis, assuming virtual point sources, indicated that the flow situation should have little effect on the entrainment coefficient. However, for real (volume) sources, no unique coefficient, valid for both jets and plumes, has been found. Reported values of the empirical constant have varied substantially (2).

Usually, when evaluating the rate of entrainment, a Gaussian lateral velocity distribution is assumed:

$$u = u_m \exp\left(-\frac{r^2}{2\sigma^2}\right) \quad \ldots\ldots\ldots\ldots\ldots (21)$$

in which $\sigma$ is the standard deviation of the velocity distribution.

The entrainment coefficient $\alpha'$ is defined by:

$$\frac{dq}{ds} = \alpha' 2\pi (\sqrt{2}\sigma) u_m \quad \ldots\ldots\ldots\ldots\ldots (22)$$

in which $\sqrt{2}\sigma$ is a characteristic length defined by the velocity profile. The relationship between the mean velocity, $\frac{m}{q}$, and the the centerline velocity, $u_m$, is as follows:

$$\frac{m}{q} = \frac{u_m}{2} \quad \ldots\ldots\ldots\ldots\ldots\ldots (23)$$

Thus empirical values of $\alpha'$ can be transferred into equivalent $\beta$ values.

Albertson (5) gives a value of $\alpha'$ of 0.057 and $\beta$ of

0.082 for a three-dimensional jet. This solution is based on constant $\beta$ values and assumes the overall mixing is completely jet-like.

For a three-dimensional jet in a homogeneous environment, Cederwall (2) presented the following solutions for a volume source:

$$\frac{q}{q_o} = \left(\frac{\beta 4}{\pi}\right)^{0.5} \frac{s}{D} \quad \ldots\ldots\ldots\ldots\ldots\ldots \quad (24)$$

$$\beta = 0.082 \quad \text{(from Albertson)(5)}$$

This equation is readilly derived using Eq. 20 and the condition: $m = m_o$.

A measure of the jet width can be related to the jet gross variables. Thus the jet radius for a round jet is given by:

$$\ell = \frac{q}{\sqrt{\pi m}} \quad \ldots\ldots\ldots\ldots\ldots\ldots \quad (25)$$

Then, $\ell = 2\sigma$ if the lateral velocity distribution is Gaussian.

2.1.3 Momentum Jets in Horizontal-Crested Expansions

In horizontal-crested expansions, the momentum jet issuing from the inlet at the base of the expansion is unable to draw on a quiescent source due to the expansion walls. Because of this, there should be no appreciable increase in the width of the jet with distance from the inlet.

The sketch (just below) indicates the fundamental difference between the two situations:

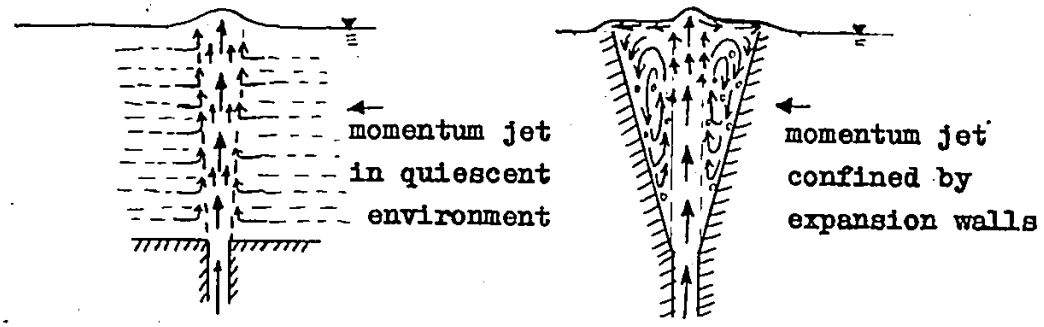


For the linear expansion indicated in this sketch, the water circulating between the edge of the jet and the expansion walls may add to the volume flux, but is generally moving in the pattern indicated and, at times, drawing in or entraining air from the top of the expansion. Linear expansions, with large internal angles and of signifigant length, would not have the same "short-circuting" effect on the momentum jet as there would be a sufficient volume of water to draw on between the jet and the expansion walls.

Equation 24 (using Albertson's value for $\beta$) implies that the flow rate would be almost doubled from the inlet to a point where s/D is 6. Eq. 25 implies that, for a doubling of the flow rate, there is no increase in the jet width for a pure momentum jet. These equations are designed to be applied to much larger scale situations than this investigation of linear expansions. For a point where s/D is 12, the flow rate would be almost four times that at the inlet and the jet width would be approximately double that of the inlet.

Since little, or no, increase in jet width is expected in any of the expansions to be tested in this investigation; and, if it can be shown that the jet separates from the walls of the expansion, at a point which is not far from the inlet, then it can be assumed that the mean velocity in the approach pipe can be considered to be the signifigant velocity in calculating the theoretical rise of the water jet above the crest of the expansion.

## 2.2 Horizontal-Crested Linear Expansions.

### 2.2.1 Dome Height

In order to discharge the flow which enters the expansion, an overflow water level "h" is maintained. This level is a function of the expansion geometry and the flow rate. From basic fluid mechanics theory, one can postulate that once the rising jet passes above the overflow water level, the pressure within the 'dome' will not be signifigantly different from atmospheric pressure. Therefore, the height to which the water will rise should be a function of the square of its velocity.

As mentioned in Sec. 2.1.3, if it can be shown that the jet breaks away from the walls of the expansion at a point where the diameter is very little larger than that of the approach pipe, then the mean velocity in the approach pipe can be taken as the signifigant velocity in calculating the theoretical rise of the water jet. This rise is obtained, in the experimental situation, by subtracting the overflow water level "h" from the dome height "H", measured above the crest

of the expansion.

2.2.2 Dimensional Analysis

There are eight characteristic parameters involved in an investigation of the performance of linear expansions. The physical properties of the expansion are fully described by the inlet diameter "D", the expansion angle "$\alpha$", the length of the expansion measured along its axis "L", and the roughness of the expansion walls "k". The parameters describing the fluid are its density "$\rho$" and the dynamic viscosity "$\mu$". The remaining two parameters are the flow rate "Q" and the gravitational acceleration constant "g". Instead of Q, the average velocity "$\bar{V}$" was used in the analysis.

Three basic quantities, having independent dimensions, - $\rho$, D, and $\bar{V}$ - were selected and the dimensional analysis was completed to yield five dimensionless numbers. The dome height "H" is a property of these five dimensionless numbers:

$$H = \phi\left(\alpha, \frac{L}{D}, \frac{k}{D}, \frac{\rho \bar{V} D}{\mu} \text{ and } \frac{\bar{V}}{\sqrt{gD}}\right) \quad \ldots\ldots\ldots (26)$$

Since the last two dimensionless numbers are the Reynold's and Froude Numbers respectively, this relationship can be written:

$$H = \phi'\left(\alpha, \frac{L}{D}, \frac{k}{D}, R_e \text{ and } F_n\right) \quad \ldots\ldots\ldots (27)$$

A further refinement can be made to Eq. 27, since the flow situation in the expansion will be fully turbulent for

the range of discharge values under investigation. Therefore, the viscosity, and hence the Reynold's Number, is no longer a governing parameter (dimensionless number). A similar comment can be applied to the roughness "k" and therefore, the dimensionless number, k/D, can be eliminated from Eq. 27.

2.2.3 Scaling Analysis

Sec. 2.2.2 has indicated that there are five dimensionless numbers describing the performance of horizontal-crested, linear expansions. From these numbers, certain relationships can be derived which indicate the necessary scaling factors governing the characteristic parameters in the transition from model to prototype conditions.

In this model analysis, the symbol, $n_x$, refers to the ratio of the magnitude of parameter x in the prototype to the magnitude of parameter x in the model. Therefore, if the diameter of the inlet pipe in the prototype is 30 centimetres, and the diameter of the inlet pipe in the model is 7.5 centimetres, then $n_D$ would be four.

From the dimensionless number L/D, the following relationship must be satisfied:

$$n_L = n_D \quad \ldots\ldots\ldots\ldots\ldots\ldots \quad (28)$$

Similarly, for the other four dimensionless numbers:

$$n_k = n_D \quad \ldots\ldots\ldots\ldots\ldots\ldots \quad (29)$$

$$n_\alpha = 1 \quad \ldots\ldots\ldots\ldots\ldots\ldots \quad (30)$$

$$n_\rho n_{\overline{V}} n_D = n_\mu \quad \ldots\ldots\ldots\ldots\ldots\ldots \quad (31)$$

$$\text{and} \quad n_{\overline{V}} n_{\overline{V}} = n_g n_D \quad \ldots\ldots\ldots\ldots\ldots\ldots \quad (32)$$

Obviously, $n_g$, $n_\rho$ and $n_\mu$ are all equal to one here; therefore, Equations 31 and 32 become:

$$n_{\overline{V}} n_D = 1 \quad \ldots\ldots\ldots\ldots\ldots\ldots \quad (33)$$

$$\text{and} \quad n_{\overline{V}} n_{\overline{V}} = n_D \quad \ldots\ldots\ldots\ldots\ldots\ldots \quad (34)$$

Clearly, Equations 33 and 34 represent conflicting situations. However, as mentioned in Sec. 2.2.2, for large values of the Reynold's number, viscosity is no longer a a governing variable, so only Equation 34 applies.

Adapting the above relationships to the flow rate, Q, results in:

$$n_Q = n_D^{2.5} \quad \ldots\ldots\ldots\ldots\ldots\ldots \quad (35)$$

## 2.3 Horizontal-Crested Bellmouths

Bellmouths have been used as inlet structures to service reservoirs. Sellin (1) investigated the performance of two bellmouth expansions and a straight pipe extension. The shapes that Sellin tested are shown in Fig. 5.

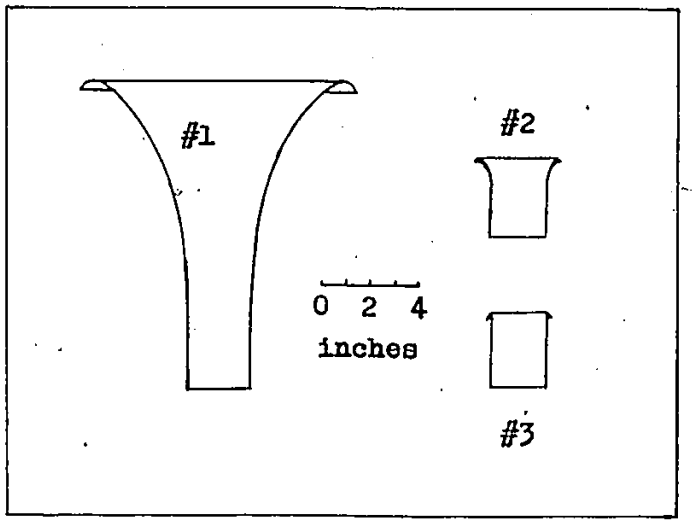


Fig. 5 - Cross-sections of Bellmouths Investigated by Sellin(1).

Figure is after Sellin(1)

Sellin suggested the use of a multi-stage cascade in conjunction with the bellmouth expansion as a means of more thoroughly aerating the water entering service reservoirs.

In the investigation, the fountain or "dome" height was defined as the level above the crest of the expansion to which the water rose for an estimated 10 per cent of the time. Measurements were made using a pointer gauge fitted with a horizontal knife-edge that was lowered until the dome height (estimated) was reached.

Experimental values of the ratio of the maximum dome height, H, to the kinetic energy of the flow in the approach pipe are presented as Fig. 7 , for the three inlet structures investigated by Sellin. Fig. 6 presents the same data with the maximum dome height, H, adjusted for the overflow head, h. Sellin was also able to make two measurements for a full-scale, 12 inch diameter (at inlet) bellmouth with the same shape as the #2 inlet shown in Fig. 5 . All of this data in Figures 6 and 7 is plotted against the Froude number. It should be noted that Sellin has represented the Froude number in the form: $\overline{V}^2/gD$, while this investigation of horizontal-crested linear expansion presents the data for maximum dome height with the Froude number in the form: $\overline{V}/\sqrt{gD}$.

Sellin concluded that it should be possible to predict the dome height for the bellmouths tested to within ± 10 per cent. For bellmouths #1 and #2, Sellin suggested that extrapolation to values of $F_n$ greater than 4 is possible since the values of $(H - h)/\overline{V}^2/2g$ approach unity with increasing discharge.

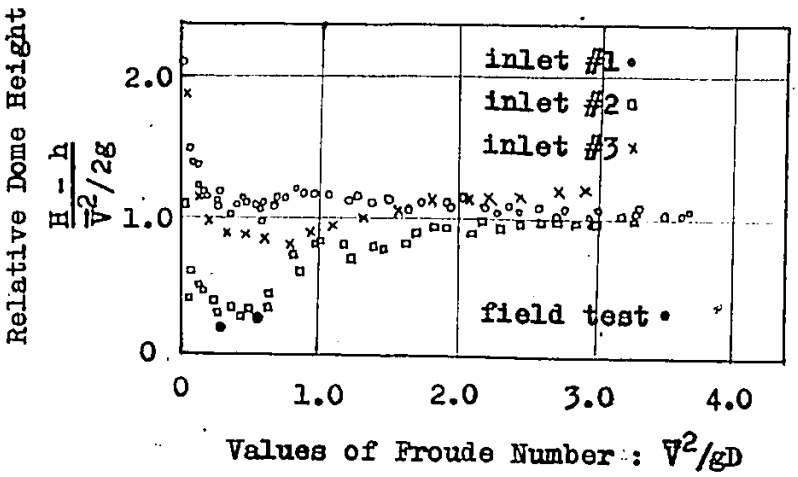


Fig. 6 - Variation of $\frac{(H - h)}{\overline{V}^2/2g}$ with $F_n$.

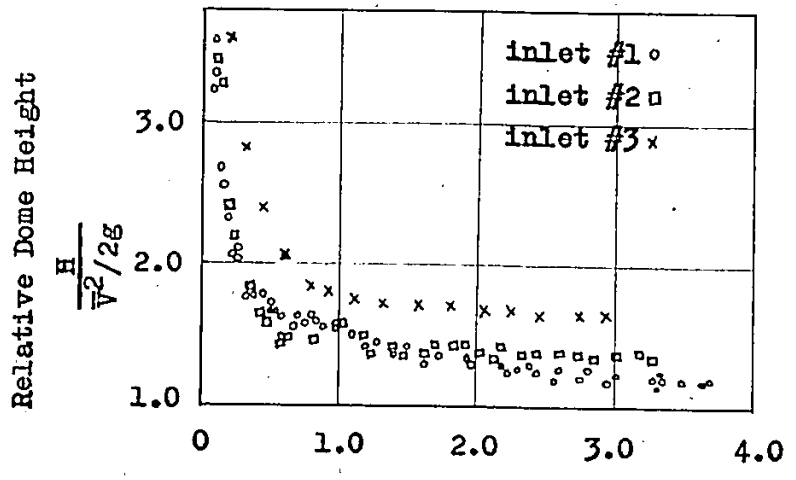


Fig. 7 - Variation of $\frac{H}{\overline{V}^2/2g}$ with $F_n$.

Figures are after Sellin (1)

# CHAPTER 3

## EQUIPMENT AND PROCEDURES

In this Chapter, the equipment used and the procedures adopted to carry out the studies will be presented.

### 3.1 Relationship of Tests to the Theory

As mentioned in Chapter 2, there are essentially three dimensionless numbers which are sufficient to fully describe the performance of the horizontal-crested, linear pipe expansions for fully-developed turbulent flow conditions. These are:

$$\alpha \quad , \quad \frac{L}{D} \quad , \text{ and } \quad \frac{\bar{V}}{\sqrt{gD}} \quad ; \text{ where:}$$

$\alpha$ is the expansion angle,

$L$ is the length of the expansion,

$D$ is the inside diameter of the inlet pipe,

$\bar{V}$ is the average velocity in the inlet pipe,

and $g$ is the gravitational acceleration constant.

Four expansion angles were selected, namely: 7, 20, 33 and 45 degrees. In addition a straight pipe extension and bellmouth expansion were investigated. These expansions' internal dimensions and shape are indicated in Figure 3 (page 8). The inside diameter of the inlet pipe was 7.82 $\pm$ 0.05 cm. Accordingly, the expansions all had the same inlet diameter providing, of course, for slight variations ($\pm$ 0.13 cm).

The inside diameter of the inlet pipe was fixed, therefore, the dimensionless ratio, L/D, was altered by cutting the expansions to one-half of their constructed length of 45.7 ± 0.24 cm. The bellmouth expansion and the straight pipe were tested for the full-length situation only.

For each expansion tested, a range of values of the dimensionless variable, $\overline{V}/\sqrt{gD}$ (Froude Number), was produced by altering the rate of flow in the system.

## 3.2 Laboratory Facilities

All experiments were performed in the Hydraulics Laboratory of the Civil Engineering Department at the University of Ottawa.

Testing of the expansions was undertaken in an uncovered tank (approximate dimensions: 3 by 3 by 1.3 meters high). A sketch of this tank, viewed from above the apparatus, is presented as Figure 8.

The inlet pipe entered the tank horizontally, just above the floor of the tank. Approximately one-half meter inside the tank wall, the pipe contained a 90 degree turn, directing the flow upwards toward the expansions. One meter above this turn the expansions were attached for testing. This one meter section of pipe contained a 30 cm long flow-straightener and wire mesh screening to dampen the effects of the abrupt turn. The flow-straightener was an "X-shaped" unit constructed from 0.32 cm plexiglass sheeting with the wire mesh screening attached at each end.

## SCHEMATIC VIEW OF APPARATUS

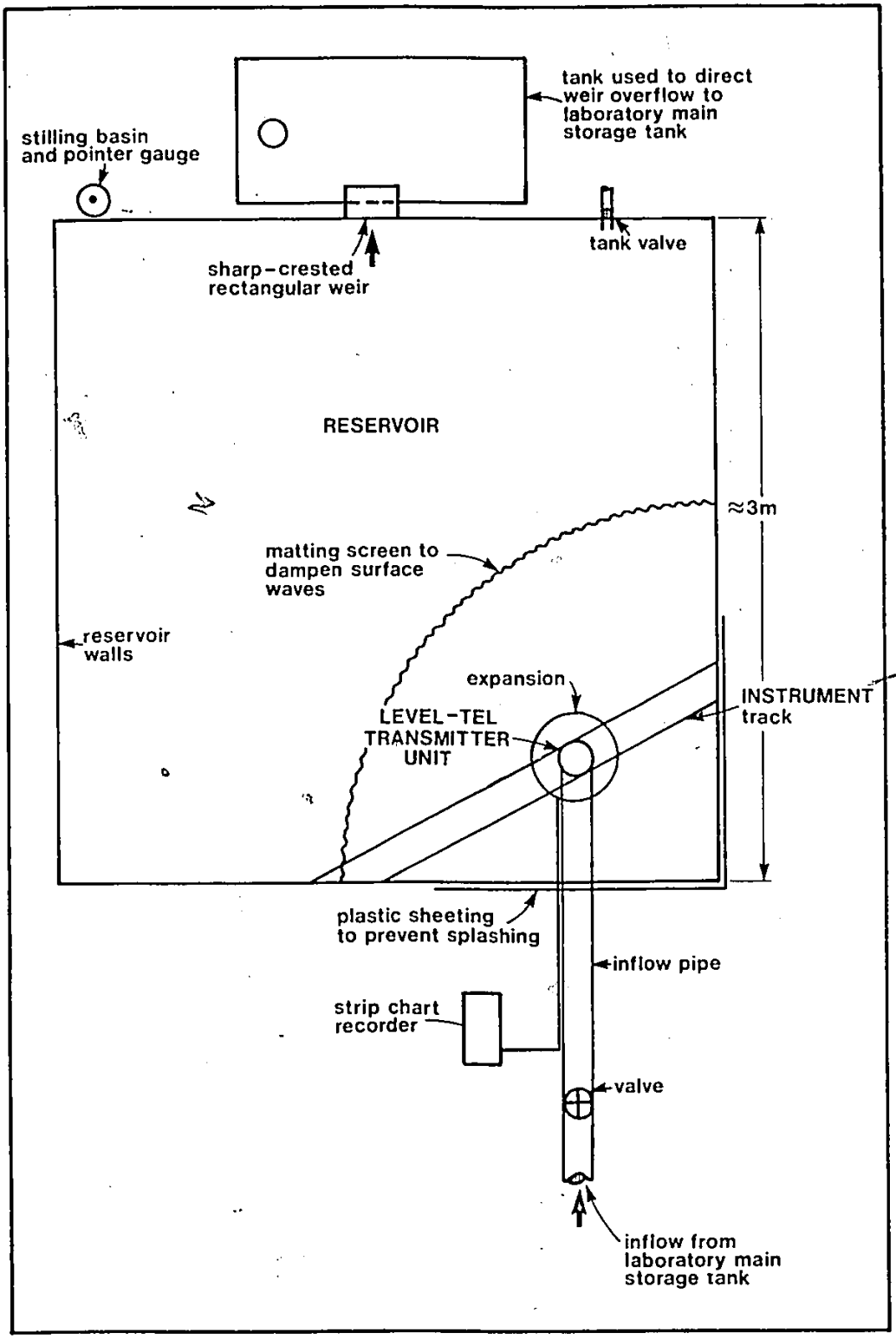


Figure 8

The vertical riser pipe was rigidly mounted, by metal restraints, to the base and sides of the tank. This prevented movement of the expansions during testing and minimized vibrations.

An instrument carriage, constructed of aluminum angle beams, was independently supported over the tank and crossed vertically above the expansion structures. A model 157-B Level-Tel transmitter was mounted on this carriage. The Level-Tel, a capacitance sensing system, provided continuous water level records when interfaced with a Hewlett Packard strip-chart recorder. Photographs of these instruments are included as Plates 1,2 and 3. The instrument carriage could be adjusted vertically and to some extent on the horizontal plane in order to place the tip of the probe at the elevation of the crest of an expansion and at any desired location in the overflow profile.

Measurement of the rate of flow through the system was facilitated by a sharp-crested, rectangular weir located in one sidewall of the tank. A stilling basin with a pointer gauge was used to measure the head of water upstream of the weir. The weir was located on the wall opposite to the one which the riser pipe assembly was near. In order to reduce the turbulence near this weir, a quarter-circle of coarse screening with a fibrous matting surrounded the riser pipe (see Figure 8 ).

Water passing over the weir was returned to the main storage tank below the laboratory floor and eventually

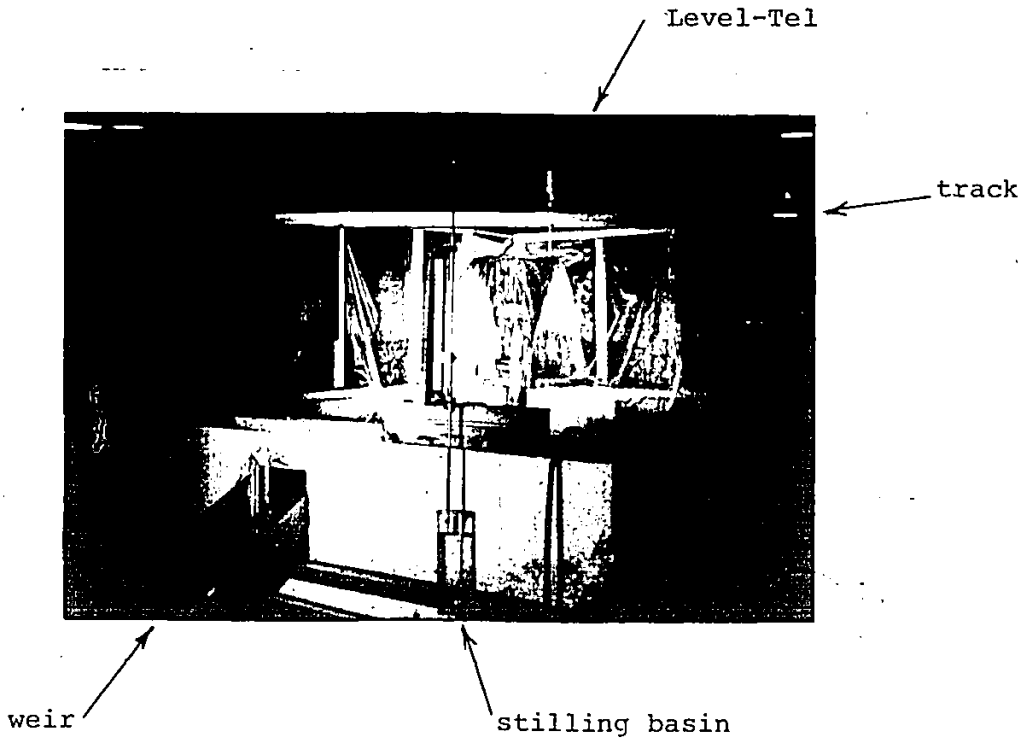


Plate 1. - Apparatus (General View)

This photograph displays most of the apparatus. The Level-Tel probe is on the track, over the $33^0$, 45.7 cm expansion. The activity indicated here is the calibration of this expansion to yield the discharge relationship shown in Fig. 11. A pointer gauge and stilling basin are in the foreground. The sharp-crested, rectangular weir is at the lower left of the photograph. The strip chart recorder was located behind the tank with the valve controlling the discharge.

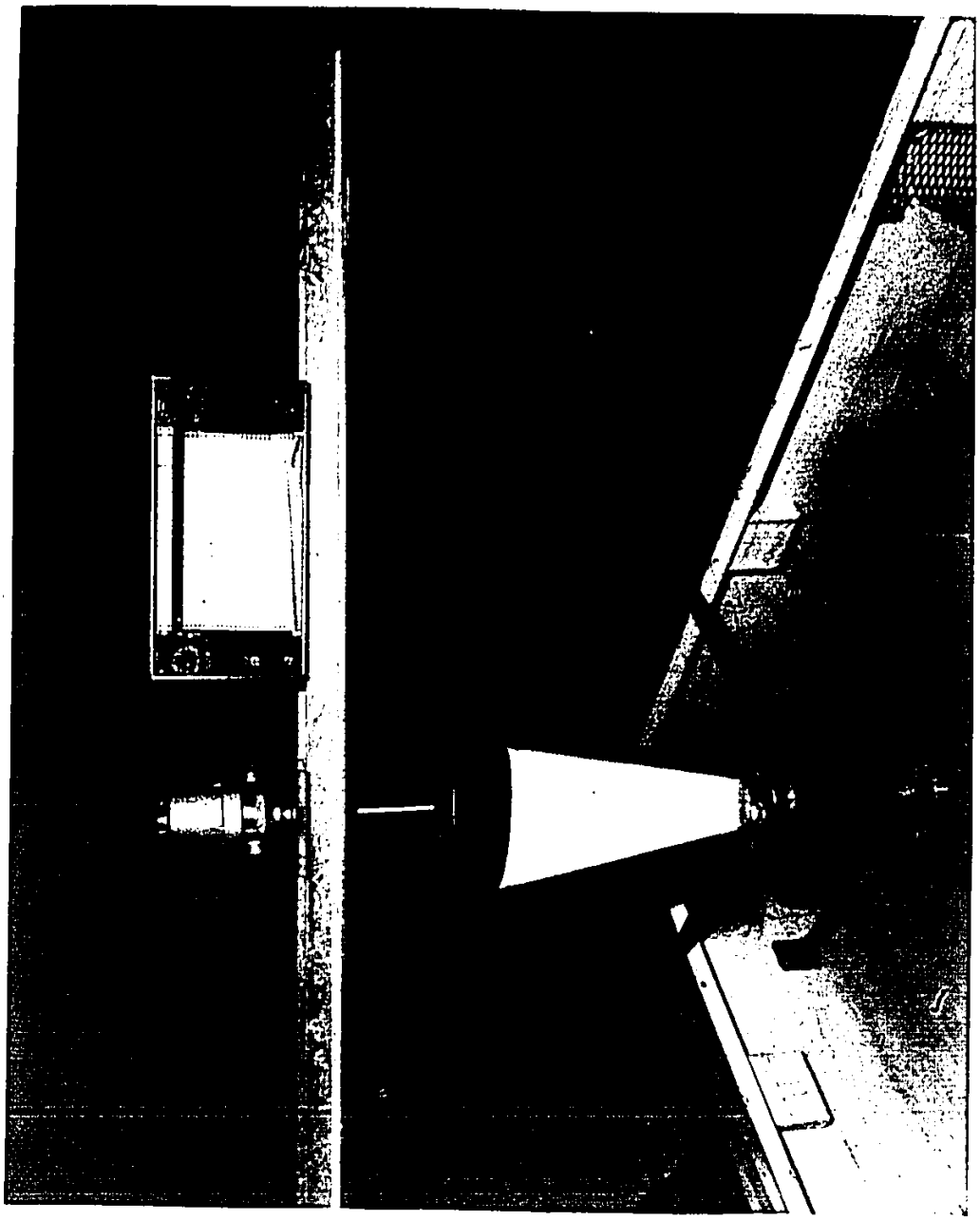

Plate 2 - Apparatus (Selected)

This plate shows the Level-Tel and the strip chart recorder on the track. Below the Level-Tel probe is the $20^0$, half-section expansion.

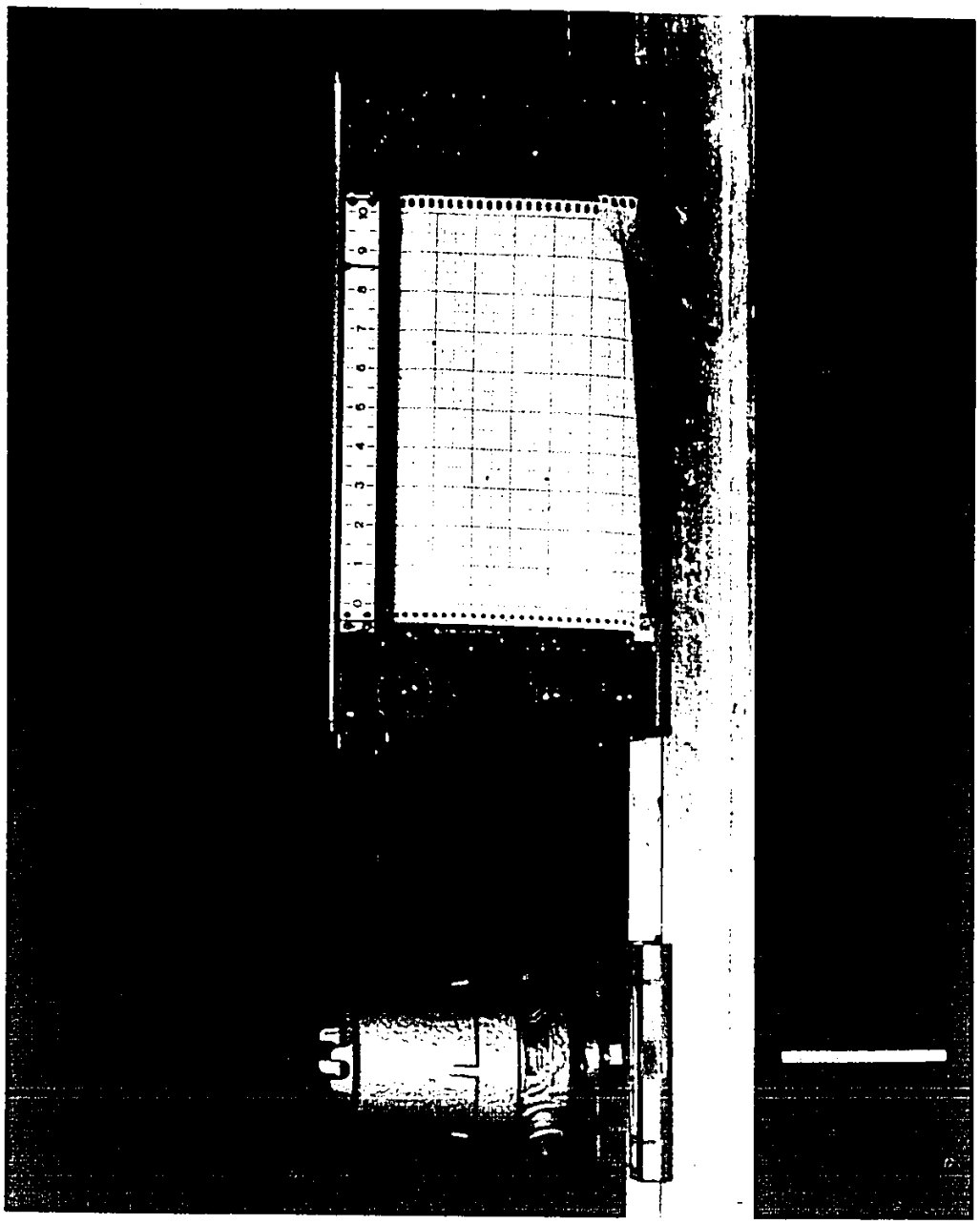

Plate 3 - Apparatus (Level-Tel and Strip Chart Recorder)

was recycled through the apparatus.

In addition to the four linear expansions, the straight pipe and the bellmouth expansion, four more linear expansions were constructed. These other expansions had identical angles as the first group discussed earlier, however, they were semi-circular in cross-section and had flat plexiglass plates on the plane of the axis. The transparent plates permitted the viewing and photography of the flow patterns in the expansions when a tracer dye was injected into the incoming supply line. Potassium permanganate, in a concentrated solution, was fed from a storage reservoir located about two meters above the crest of the expansions in these particular studies.

## 3.3 Calibration of the Apparatus

### 3.3.1 The Weir

Measurement of the rate of flow of water through the expansions was provided by determining the height to water level above the crest of the sharp-crested rectangular weir. The head (h) was obtained from the stilling basin and pointer gauge assembly. This measurement was then input to a rating curve to obtain the flow rate.

The rating curve (Figure 9.) was prepared from 24 measurements. The flow rate was obtained by determining the weight of water which accumulated in a tank in a measured amount of time. An Avery scale, with a capacity in excess of 500 kg, and a stop watch with 0.2 second indications were

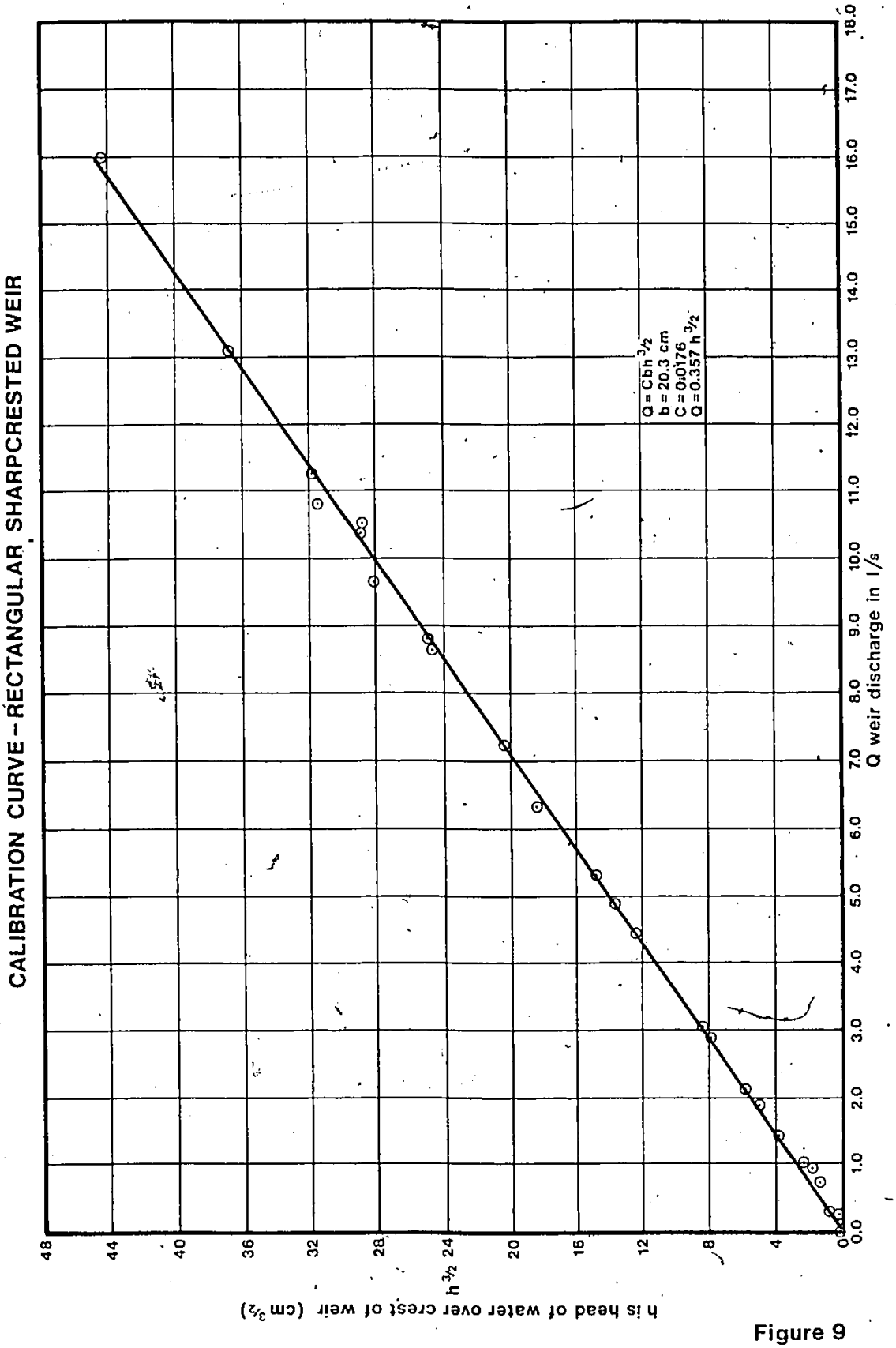
CALIBRATION CURVE - RECTANGULAR SHARPCRESTED WEIR
Q = Cbh 3/2
b = 20.3 cm
C = 0.0176
Q = 0.357 h 3/2
Q weir discharge in l/s
h is head of water over crest of weir (cm 3/2)
h 3/2
0.0
1.0
2.0
3.0
4.0
5.0
6.0
7.0
8.0
9.0
10.0
11.0
12.0
13.0
14.0
15.0
16.0
17.0
18.0
0
4
8
12
16
20
24
28
32
36
40
44
48

Figure 9

used. For each observation, the weight and time were read three times and averaged.

The most important procedure for all flow measurements taken for this experiment was that the water level in the tank had to be given adequate time to achieve a steady position. For low flows this could easily take five or more minutes.

### 3.3.2 The "Level-Tel" Transmitter

The calibration of the Level-Tel transmitter, (interfaced with the Hewlett Packard strip-chart recorder), was accomplished using a tank full of water. The tank had a valve near its base. A pointer gauge was used to measure the water level in the tank.

The probe was immersed to a depth of approximately 15 cm. After the surface fluctuations had stopped, a pointer gauge reading and the voltage indicated on the Hewlett Packard recorder were noted. Little by little, the tank was drained and 65 sets of readings were taken. The resulting calibration curve is presented as Figure 10.

It is interesting to note that this curve is linear for the range of 2 to 13.5 cm of water over the tip of the probe. Above 13.5 cm, the probe would not provide any increase in output signal.

This calibration was checked on two other occasions during the course of the experimental work and no deviation from the original curve was observed.

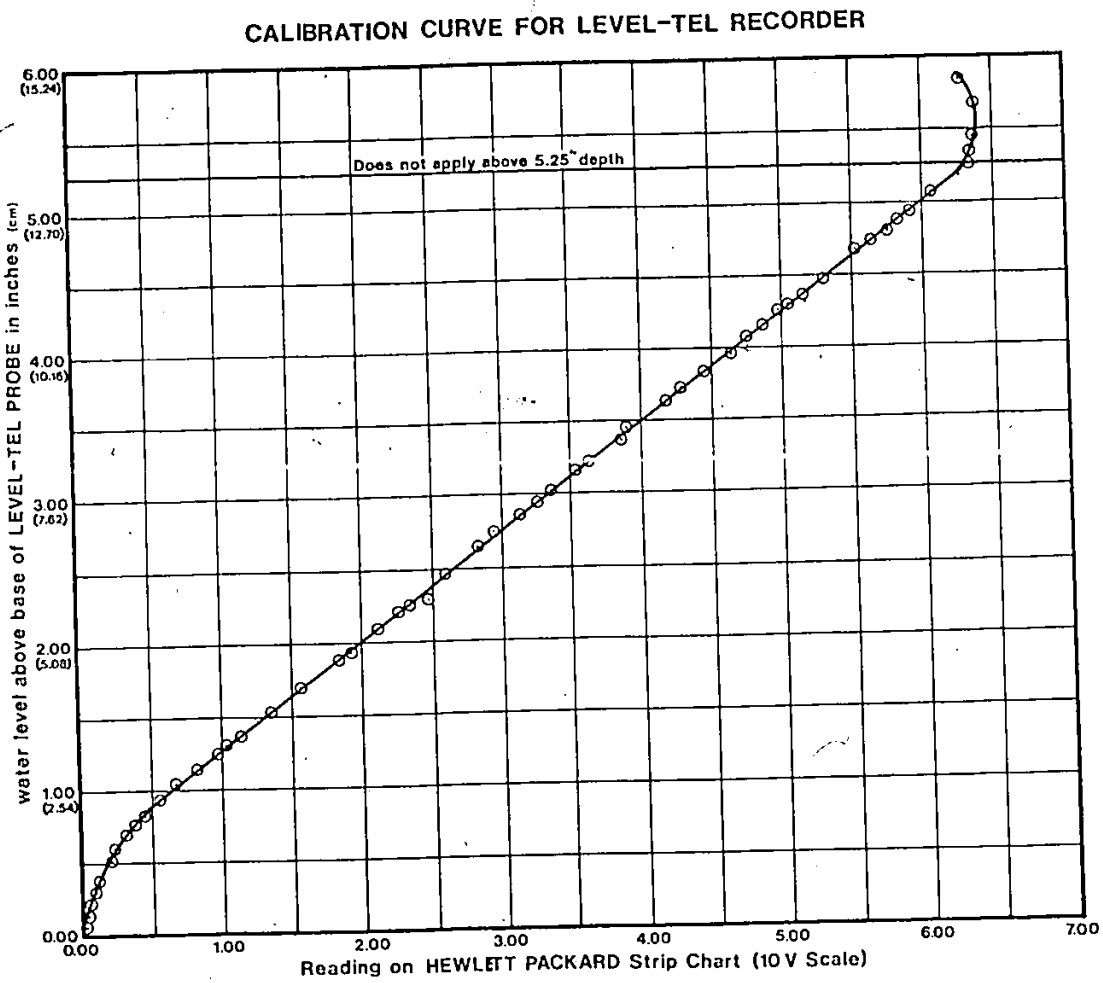
CALIBRATION CURVE FOR LEVEL-TEL RECORDER
Does not apply above 5.25" depth
water level above base of LEVEL-TEL PROBE in inches (cm)
6.00 (15.24)
5.00 (12.70)
4.00 (10.16)
3.00 (7.62)
2.00 (5.08)
1.00 (2.54)
0.00
0.00
1.00
2.00
3.00
4.00
5.00
6.00
7.00
Reading on HEWLETT PACKARD Strip Chart (10 V Scale)

Figure 10

# CHAPTER 4

## PRESENTATION AND DISCUSSION OF RESULTS

### 4.1 Expansion Overflow Discharge Relationships

In all, ten expansions were investigated. These were the straight pipe, bellmouth, 7°, 20°, 33° and 45° full-length expansions (45.7 cm long); and the 7°, 20°, 33° and 45° half-length expansions (22.8 cm long). For each of these expansions a relationship of overflow water level "h" as a function of discharge was required.[1] The straight pipe was not cut in half for testing as it was assumed that the performance should be identical for both the 45.7 and 22.8 cm lengths.

Figures 11 and 12 indicate the data and the accepted relationships for the overflow water level "h" as a function of discharge. For each expansion, the discharge was gradually stepped up until the water surface in the expansion was too rough to enable suitably accurate data to be measured. In cases where surface turbulence was too severe to define an overflow discharge relationship, a damping device was inserted in the expansion. A standard soil grain-size sieve filled with machine-bolt nuts served this purpose well (see Plate 4).

As expected, the discharge is a function of the overflow water level "h" raised to the power 1.5:

$$Q = f(h^{1.5})$$

For small discharges and for the larger expansions in particular,

---

[1] this relationship was required so 'h' could be determined under high flow situations when 'h' was not readilly measurable.

## HEIGHT OF WATER OVER CREST OF EXPANSION UNITS VERSUS DISCHARGE (45.7 cm expansion)

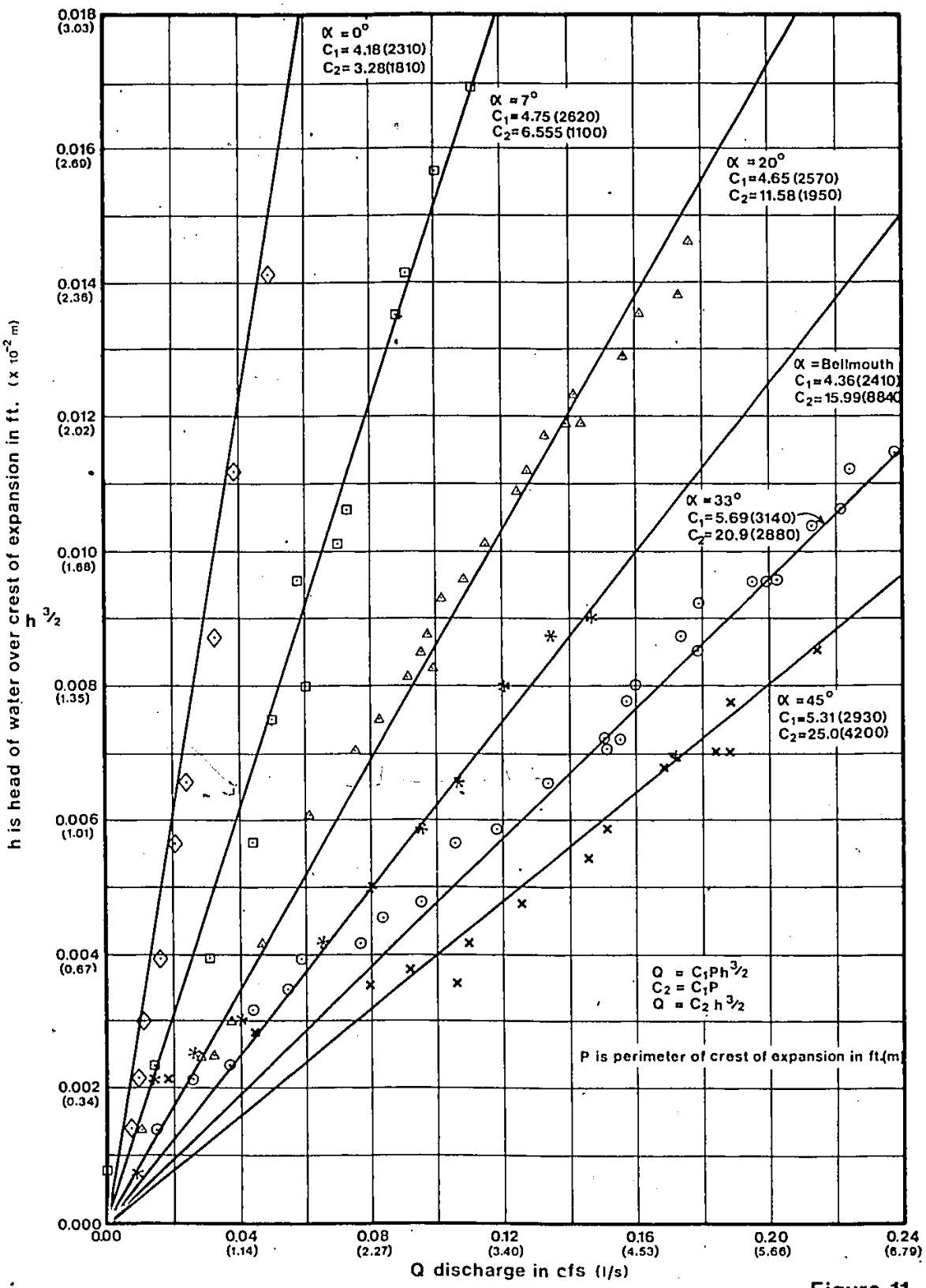


Figure 11

## HEIGHT OF WATER OVER CREST OF EXPANSION VERSUS DISCHARGE (22.8 cm expansions)

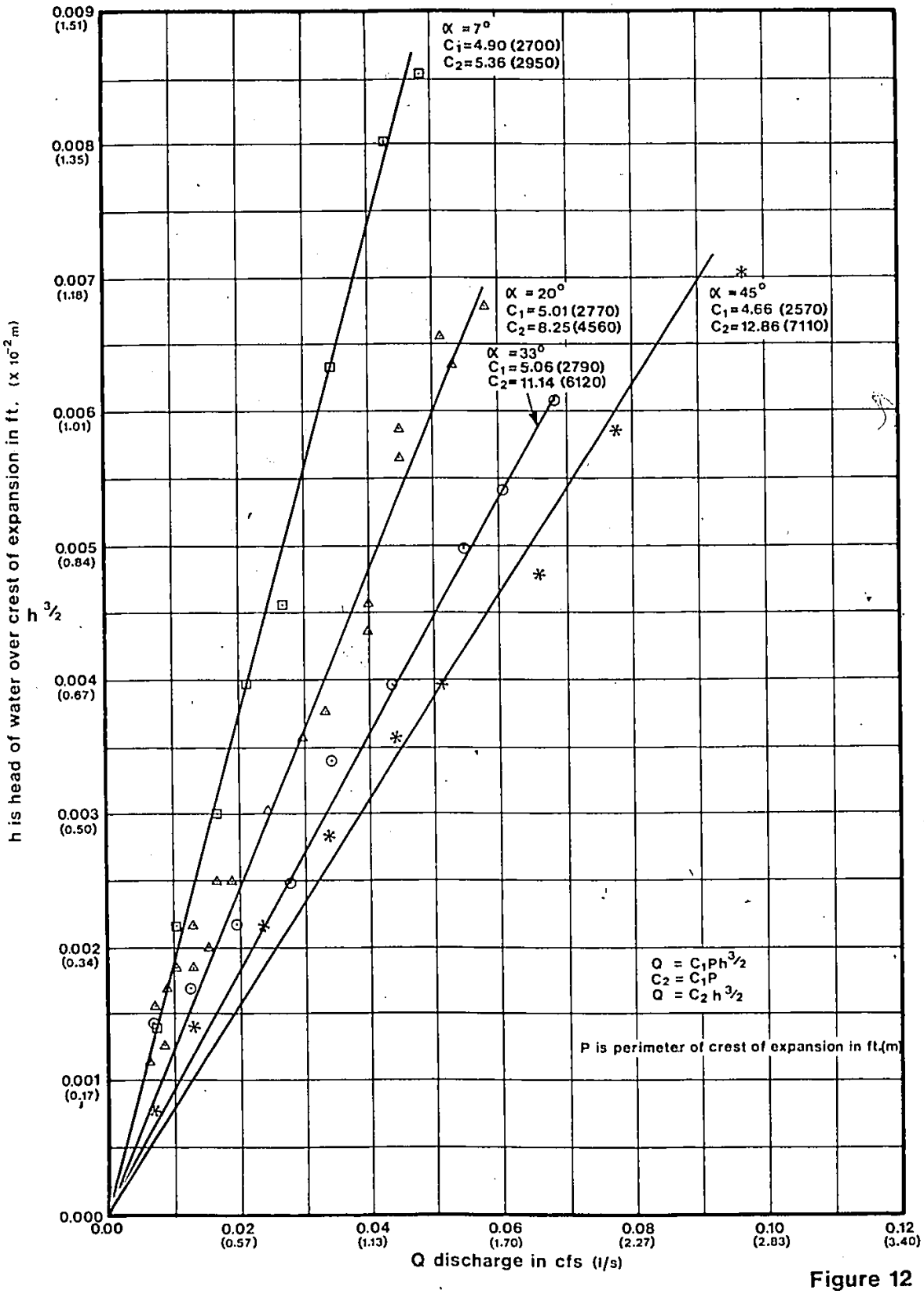


Figure 12

Plate 4. - Calibration of the $33^0$, 45.7 cm Expansion.
(With sieve in place) (Q = 5.72 l/s)

the deviation from this relationship is due to the attractive forces between the water and the expansion material and to the surface tension of the water.

The general equation for overflow discharge in this situation is:

$$Q = C_1 P h^{1.5}$$

where: Q is the overflow discharge

$C_1$ is the discharge coefficient, and

P is the perimeter of the crest of the expansion.

As a matter of convenience, $C_1$ and P were combined into one coefficient, $C_2$:

$$Q = C_2 h^{1.5}$$

Table 1 contains the values of $C_1$ and $C_2$ for both fps and mks units.

The straight pipe had a fairly sharp crest. All of the linear expansions; with the exception of the 45.7 cm, 20° expansion, which had a partially sharpened crest; had flat crests.

## 4.2 Performance of the Expansions

Of signifigant interest to the designer using a vertical riser pipe in a service reservoir would be the knowledge of the relative performance of different expansions

Table 1. - Expansion Discharge Coefficients[1]

Full-Length Expansions (45.7cm)

| Expansion | $C_1$ | | $C_2$ | |
|---|---|---|---|---|
| | fps | mks | fps | mks |
| 7° | 4.75 | 2620 | 6.56 | 1100 |
| 20° | 4.65 | 2570 | 11.6 | 1950 |
| 33° | 5.69 | 3140 | 20.9 | 2880 |
| 45° | 5.31 | 2930 | 25.0 | 4200 |
| straight | 4.18 | 2310 | 3.28 | 1810 |
| bellmouth | 4.36 | 2410 | 16.0 | 8840 |

Half-Length Expansions (22.8 cm)

| Expansion | $C_1$ | | $C_2$ | |
|---|---|---|---|---|
| | fps | mks | fps | mks |
| 7° | 4.90 | 2700 | 5.36 | 2950 |
| 20° | 5.01 | 2770 | 8.25 | 4560 |
| 33° | 5.06 | 2790 | 11.1 | 6120 |
| 45° | 4.66 | 2570 | 12.9 | 7110 |

[1]If fps units are used, the discharge "Q" will be in cfs.
If mks units are used, the discharge "Q" will be in l/s.

and the height above the crest to which the water would rise.

Unfortunately, when one observes the fountain of water discharging from the top of an expansion, or, for that matter, a straight pipe, it becomes apparent that there is no one level for a particular discharge which can be determined to be the maximum level to which the water rises. There is, however, a level above which only detached masses of water rise which would not endanger any roof structure that they might strike. Sellin (1), found that this level was not difficult to determine but that it varied with time due to the random nature of the turbulence in the upflowing water. He made measurements using a pointer gauge fitted with a horizontal knife-edge that was lowered until the water dome reached the same level for an estimated ten per cent of the time. Accordingly, in the investigation of the linear expansions, the maximum dome height was selected as the level to which the water rose (or exceeded) for ten per cent of the time. The maximum dome height was therefore given the symbol, $H_{10}$.

A typical section of strip chart record - for the $33^{o}$, 45.7 cm expansion - is shown (Fig. 13). The abscissa represents time, in seconds, and the ordinate represents volts. The voltage is converted to the water level above the base of the Level-Tel probe using the relationship in Fig. 10.

The maximum dome height is, as indicated in Sec. 3.1, a function of three dimensionless numbers:

$$\alpha \ , \ \frac{L}{D} \quad \text{and} \quad \frac{\overline{V}}{\sqrt{gD}} \ .$$

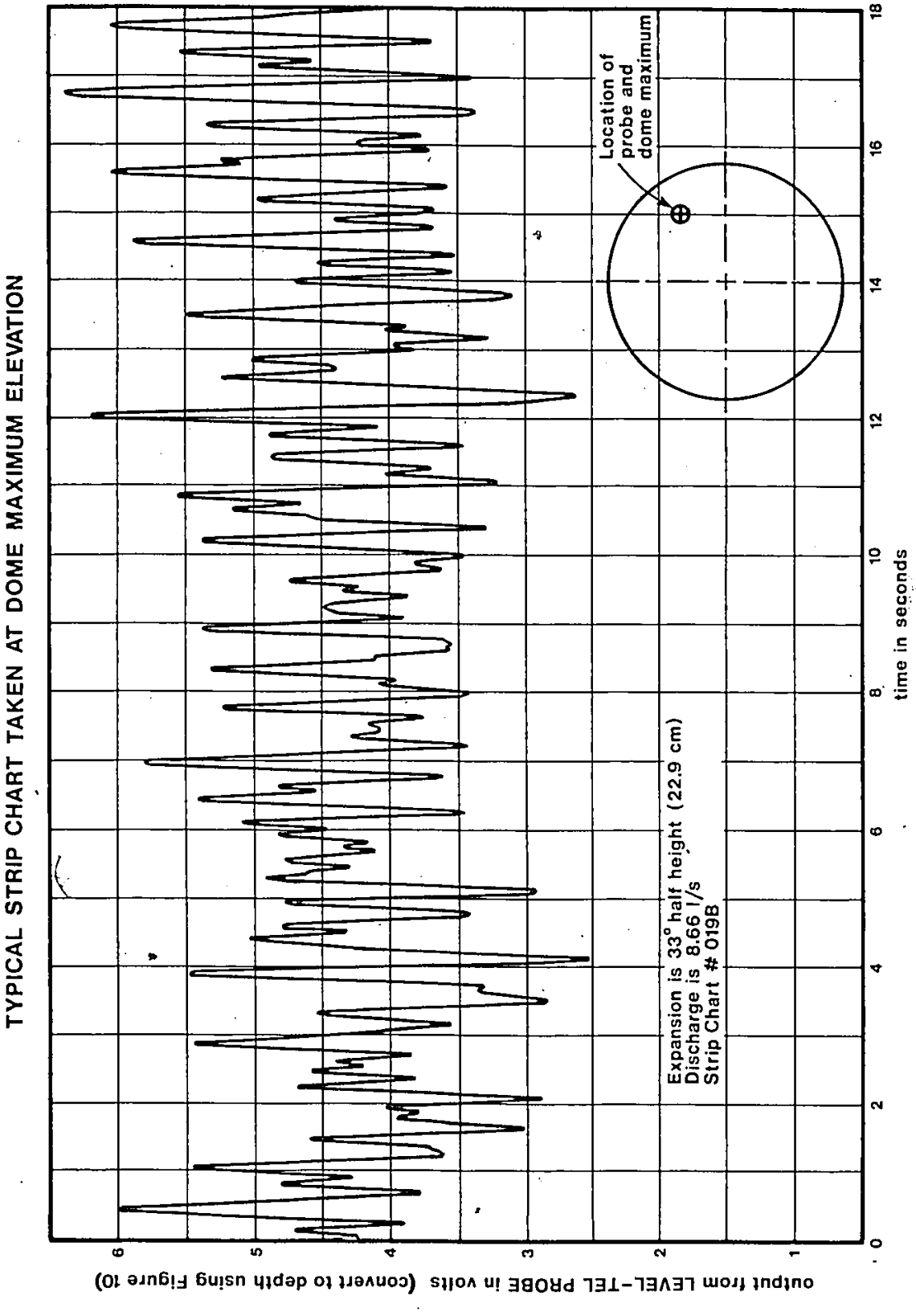
TYPICAL STRIP CHART TAKEN AT DOME MAXIMUM ELEVATION
output from LEVEL-TEL PROBE in volts (convert to depth using Figure 10)
time in seconds
Location of probe and dome maximum
Expansion is 33° half height (22.9 cm)
Discharge is 8.66 l/s
Strip Chart # 019B

Figure 13

Due to the turbulent state of flow and the very short length of time which the water particles actually are influenced by the surface roughness of the expansions, the other two dimensionless numbers:

$$\frac{k}{D} \quad \text{and} \quad \frac{\rho VD}{\mu}$$

would not have a signifigant influence on the dome height.

4.2.1 Maximum Dome Height

The variation of the maximum dome height as a function of the expansion angles, lengths and discharge is indicated in Figures 14 and 15. Fig. 14 represents the data for the 45.7 cm expansions (L/D = 5.84), while Fig. 15 presents the data for the 22.8 cm expansions for which L/D is 2.92. The abscissae represent the Froude number, $V/\sqrt{gD}$, which is essentially another way of expressing the flow rate. The ordinates are ratios of the maximum dome height to the kinetic energy of the flow at the entrance to the expansions. The maximum dome height is the level reached or exceeded ten per cent of the time.

An obvious comment which can be made on observing Figures 14 and 15 is that for the same Froude number, the half-length (22.8 cm) expansions which are signifigantly different from the straight pipe have given approximately twice the maximum dome height as the full-length expansions.

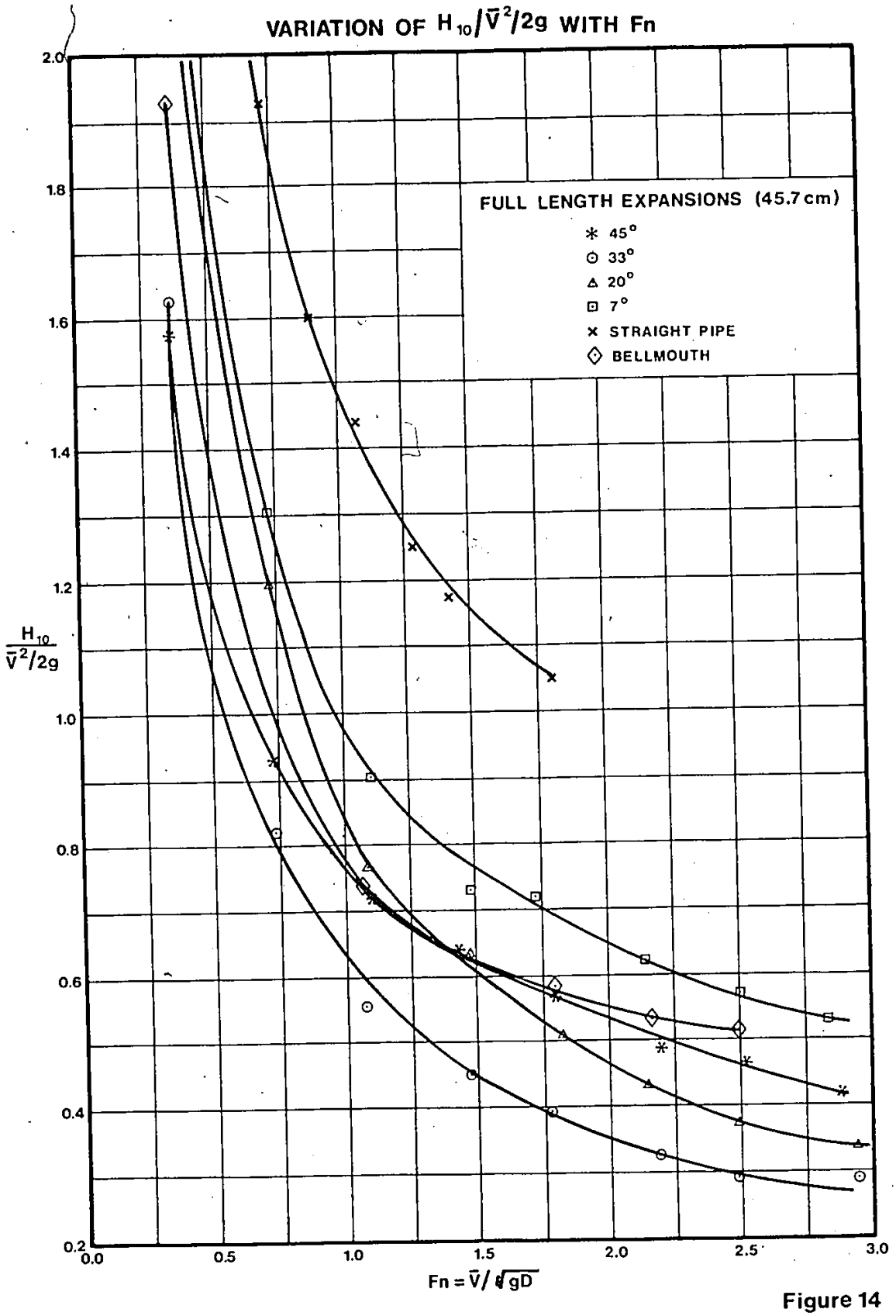
VARIATION OF $H_{10}/\bar{V}^2/2g$ WITH Fn
FULL LENGTH EXPANSIONS (45.7 cm)
45°
33°
20°
7°
STRAIGHT PIPE
BELLMOUTH
$\frac{H_{10}}{\bar{V}^2/2g}$
Fn = $\bar{V}/\sqrt{gD}$
2.0
1.8
1.6
1.4
1.2
1.0
0.8
0.6
0.4
0.2
0.0
0.5
1.0
1.5
2.0
2.5
3.0

Figure 14

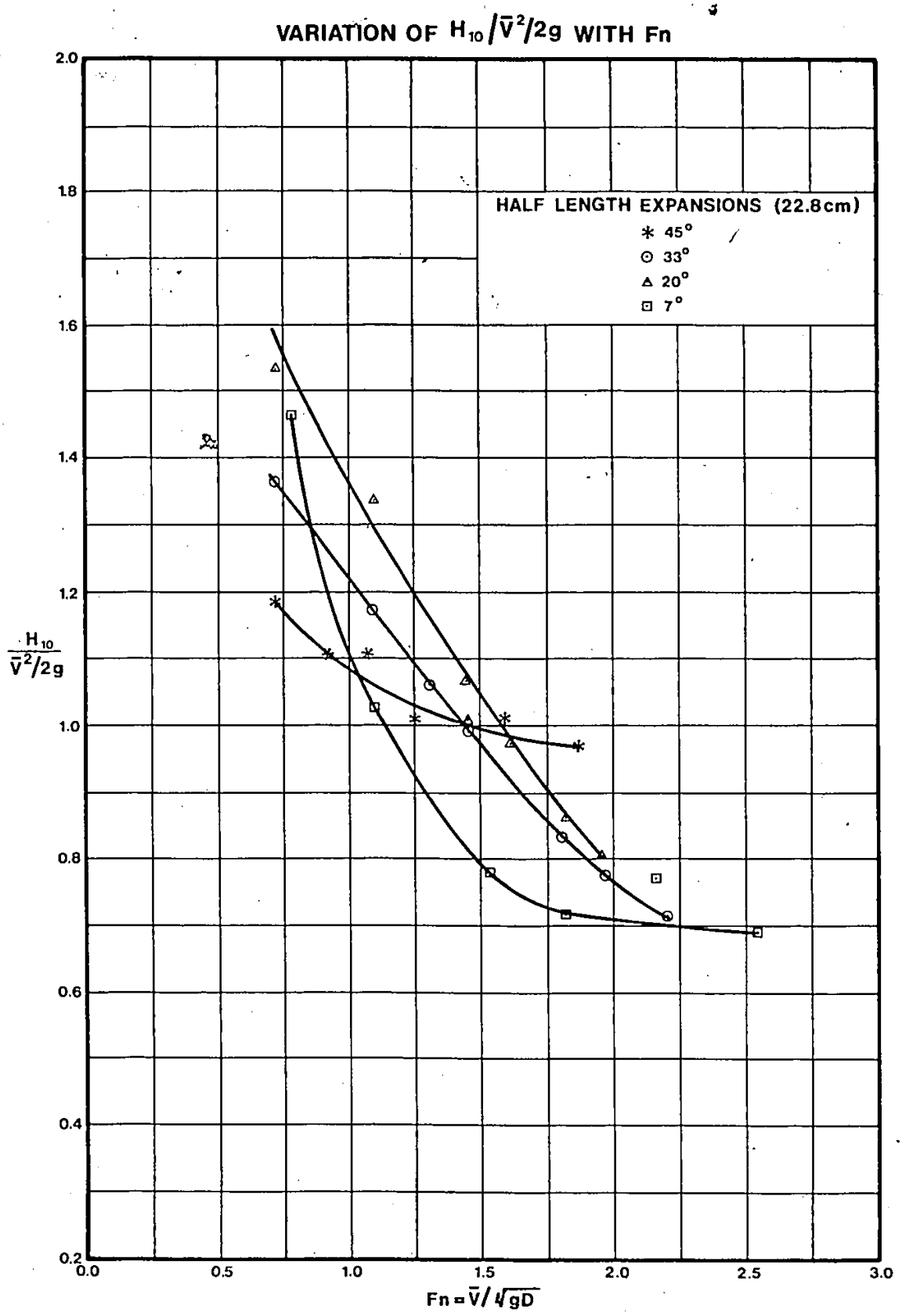
VARIATION OF $H_{10}/\bar{V}^2/2g$ WITH Fn
HALF LENGTH EXPANSIONS (22.8cm)
* 45°
⊙ 33°
△ 20°
⊡ 7°
$\frac{H_{10}}{\bar{V}^2/2g}$
2.0
1.8
1.6
1.4
1.2
1.0
0.8
0.6
0.4
0.2
0.0
0.5
1.0
1.5
2.0
2.5
3.0
$Fn = \bar{V}/\sqrt{gD}$

Figure 15

Table 2 uses data drawn from Figures 14 and 15 to support this statement. The best performance in reducing the maximum dome height with increased length is clearly obtained using the $33^{\circ}$ expansion.

As can be seen in Fig. 14, the $33^{\circ}$ expansion has a far superior performance than the bellmouth as far as the capability to reduce the maximum dome height. This is true for all observed values of the Froude number and it appears that this should be the same for Froude numbers well in excess of 3. Froude number 3.0 corresponds to a discharge of 22,700 l/s (4800 gpm) for a 30 cm diameter riser pipe.

The maximum dome height for any of the full-length (45.7 cm) expansions tested was well below the maximum height for the straight pipe. Only a slight reduction in maximum dome height was achieved for the half-length (22.8 cm) expansions compared to the straight pipe's performance. Although the $7^{\circ}$ expansion appears to be the best expansion for the 22.8 cm length (L/D = 2.92), Fig. 15 indicates that this superiority will not persist much above $F_n = 2.25$. It is also evident that there is little difference in the maximum dome height for the full-length and half-length cases using the $7^{\circ}$ expansion.

Several data points could not be plotted in Figures 14 and 15 as they fell far too high. These values are listed in Table 3.

Plates 5 to 20 and the small descriptions describe the expansions in operation.

Table 2. - Comparison of Maximum Dome Heights for Different Ratios of L/D.

Ratio: $\frac{H_{10}}{\overline{V}^2/2g}$ for L/D = 2.92 divided by $\frac{H_{10}}{\overline{V}^2/2g}$ for L/D = 5.84

| Froude No. | 1.0 | 1.5 | 2.0 | 2.5 |
|---|---|---|---|---|
| Expansion Angle | | | | |
| 7° | 1.2 | 1.1 | 1.2 | 1.2 |
| 20° | 1.7 | 1.7 | 1.7 | - |
| 33° | 2.0 | 2.1 | 2.1 | 2.2 |
| 45° | 1.5 | 1.6 | 1.6 | - |

Table 3. - Additional Data for Figures 14 and 15.

| L/D = 5.84 | | | L/D = 2.92 | | |
|---|---|---|---|---|---|
| Expansion | $F_n$ | $H_{10}/\overline{V}^2/2g$ | Expansion | $F_n$ | $H_{10}/\overline{V}^2/2g$ |
| 7° | 0.36 | 2.70 | 7° | 0.35 | 3.50 |
| 20° | 0.37 | 2.64 | 20° | 0.35 | 2.87 |
| straight | 0.38 | 3.80 | 33° | 0.36 | 2.32 |
| | | | 45° | 0.36 | 2.24 |

Plate 5. - $33^0$, 45.7 cm Expansion (Q = 5.72 l/s)

This plate shows the $33^0$ expansion at the same discharge as Plate 4; however, there is no seive inserted to damp surface turbulence.
($F_n$ = 1.45)

Plate 6. - $33^0$, 45.7 cm Expansion (Q = 5.72 l/s)

This plate shows the $33^0$ expansion at the same discharge as Plate 5; however, the dome has collapsed. ($F_n$ = 1.45)

Plate 7. - $7^0$ Expansion Under Discharge of 5.97 l/s

(Froude number is 1.51)

Plate 8. - $7^0$ Expansion (Q = 10.6 l/s)

This plate clearly indicates that the definition of the overflow water level, h, becomes pointless for expansions of small angles due to the dominance of the entire top of the expansion by the dome. ($F_n$ = 2.68)

Plate 9. - $45^0$, 45.7 cm Expansion (Q = 9.03 l/s)

Note that the dome is well-centered, as it usually was for this expansion. ($F_n$ = 2.29)

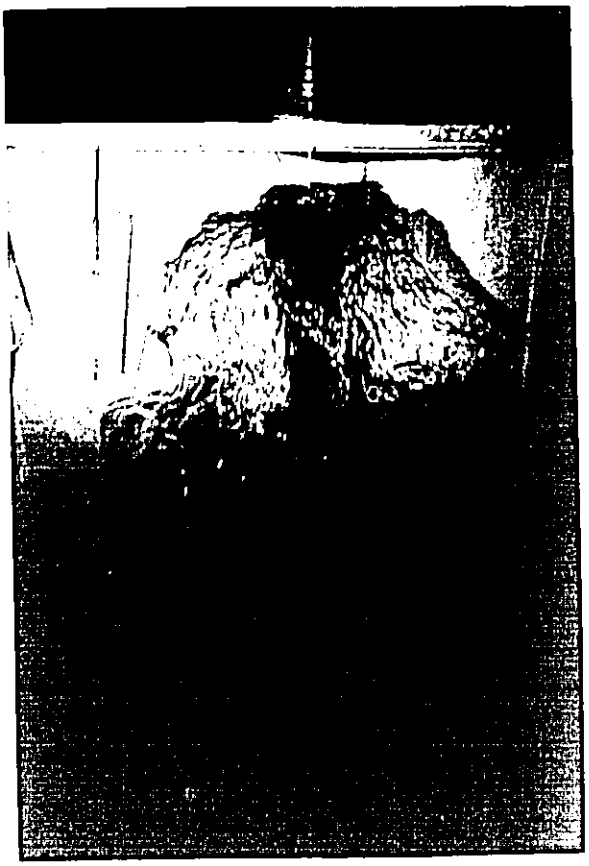

Plate 10. - Bellmouth Expansion (Q = 7.05 l/s)

The dome for the bellmouth expansion was always well-centered and rarely collapsed. There was always less fluctuations in height of the dome than for the linear expansions with the exception of the $7^0$ expansion.

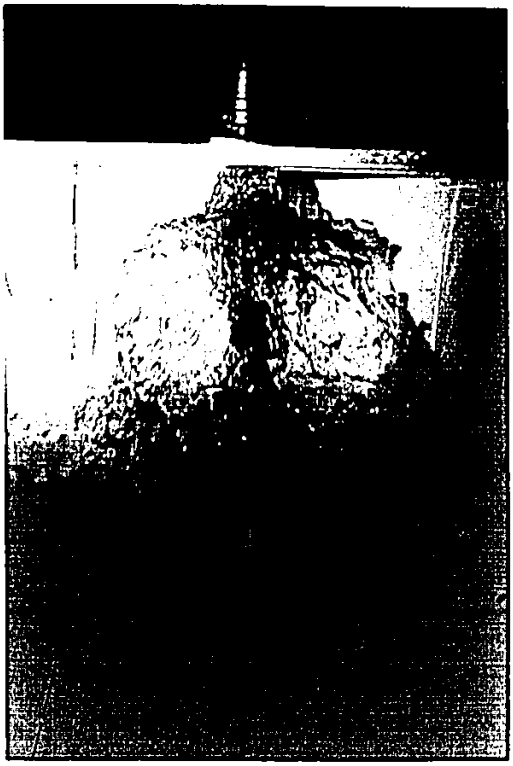

Plate 11. - Bellmouth Expansion (Q = 11.4 l/s)

The dome has extended up between the beams of the track. ($F_n$ = 2.88)

Plate 12. - Straight Pipe Extension (Q = 0.45 l/s)

This is a close-up shot of the straight pipe extension with the probe centered. ($F_n$ = 0.12)

Plate 13. - Straight Pipe Extension (Q = 4.22 l/s)

For both the straight pipe extension and the $7^0$ expansion, the probe obstructed the dome height considerably if positioned in the center of the expansion. Accordingly the data was taken with the probe as shown and slight adjustments made.

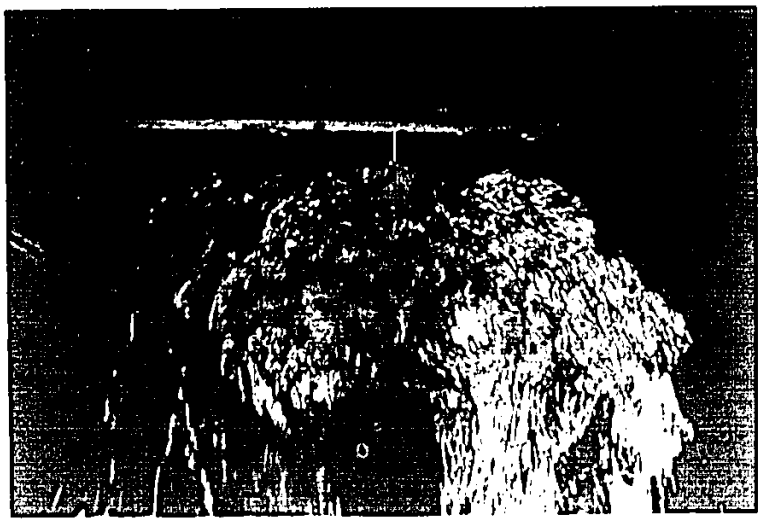

Plate 14. - Straight Pipe Extension (Q = 7.08 l/s)

Close-up shot. ($F_n$ = 1.79)

Plate 15. - $7^0$, 22.8 cm Expansion (Q = 10.0 l/s)

The domes for the half-length (22.8 cm) expansions were more turbulent than those for the full-length expansions.. ($F_n$ = 2.53)

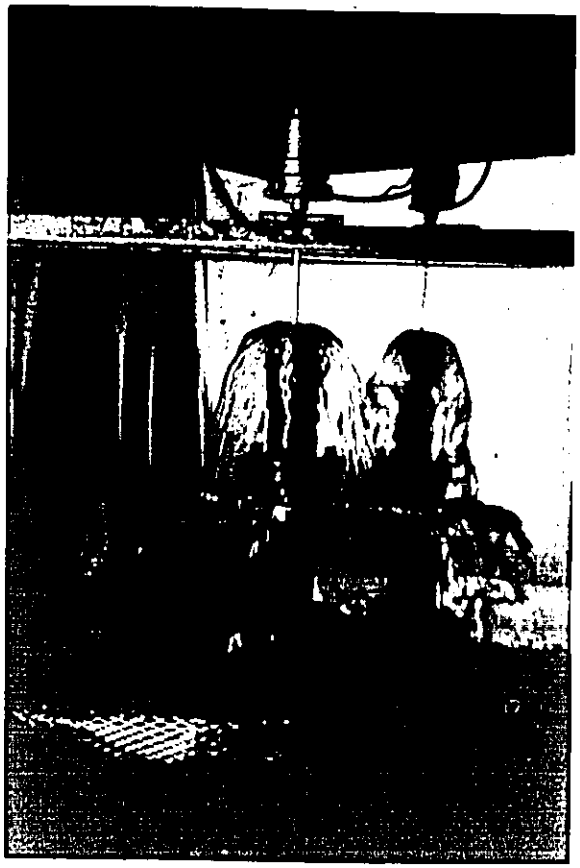

Plate 16. - $7^0$, 22.8 cm Expansion (Q = 3.06 l/s)

($F_n$ = 0.78)

Plate 17. - $33^0$, 22.8 cm Expansion (Q = 8.66 l/s)

The dome changed position frequently. The screening material, visible in the foreground, damped the surface turbulence in the tank. ($F_n$ = 2.20)

Plate 18. - $45^0$, 22.8 cm Expansion (Q = 7.33 l/s)

The dome was very turbulent, but better-centered than the $33^0$, 22.8 cm expansion. ($F_n$ = 1.86)

Plate 19. - $20^0$, 22.8 cm Expansion (Q = 4.30 l/s)

The dome would form at the center only for discharges less than 0.075 l/s. The jet could be shifted to any position around the wall by inserting a hand in the flow. ($F_n$ = 1.09)

Plate 20. - $20^0$, 22.8 cm Expansion (Q = 7.13 l/s)

($F_n$ = 1.81)

4.2.2 Energy Dissipation in Expansions

In order to determine how much energy is dissipated in the expansions tested, Figures 16 and 17 were prepared from the data points in Figures 14 and 15 and Table 3 by subtracting the overflow water level "h" from the maximum dome height. One point could not be plotted in Figure 16 ; this was a maximum dome height to kinetic energy ratio of 1.08 for the 20° expansion at a Froude number of 0.37.

The performance of the straight pipe and the 7°, 45.7 cm expansion, as presented in Fig. 16, and the 7°, 22.8 cm expansion, as shown in Fig. 17, does not seem reasonable. The 7°, 45.7 cm expansion appears to achieve a 60 per cent reduction in energy during the translation from kinetic to potential energy. This reduction is quite high. In actual fact, there should be practically no loss in energy for the straight pipe.

Plates 13 and 16, of the straight pipe at a discharge of 4.22 l/s and the 7° expansion at a discharge of 3.06 l/s, show that the overflow is subject to considerable influence from the dome itself. This implies that the dome height has considerable influence on the overflow directly and that the effective overflow levels are somewhat less than those calculated by simply extending the linear relationships plotted in Figures 11 and 12 for the straight pipe and the 7° expansion.

As a result of this problem mentioned in the previous paragraph, the data presented in Figures 16 and 17 for the straight pipe and the 7° expansion cannot be applied to design expansions with inlet diameters and lengths different from those

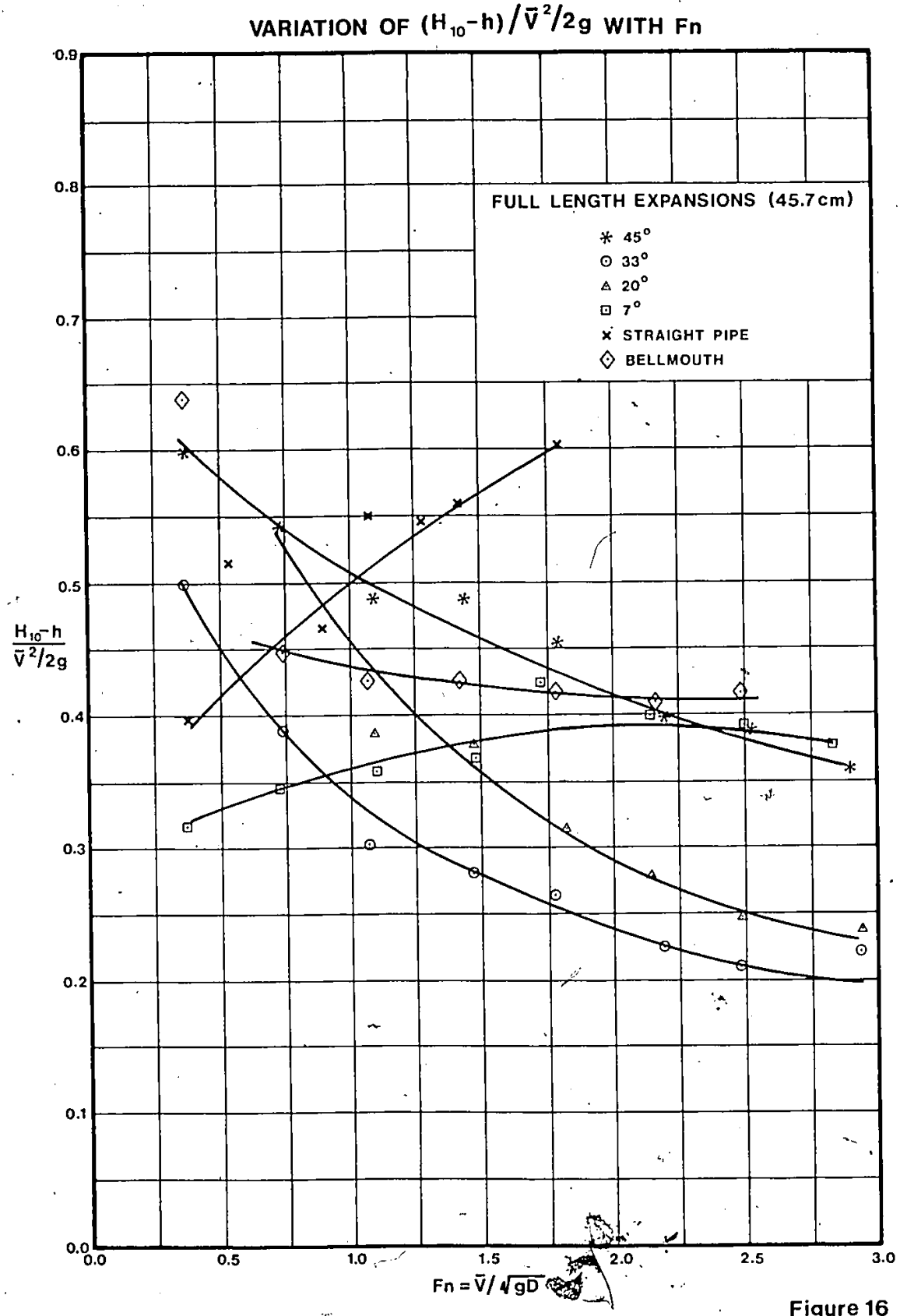
VARIATION OF $(H_{10}-h)/\bar{V}^2/2g$ WITH Fn
FULL LENGTH EXPANSIONS (45.7cm)
45°
33°
20°
7°
STRAIGHT PIPE
BELLMOUTH
$\frac{H_{10}-h}{\bar{V}^2/2g}$
0.0
0.1
0.2
0.3
0.4
0.5
0.6
0.7
0.8
0.9
0.0
0.5
1.0
1.5
2.0
2.5
3.0
$Fn = \bar{V}/\sqrt{gD}$

Figure 16

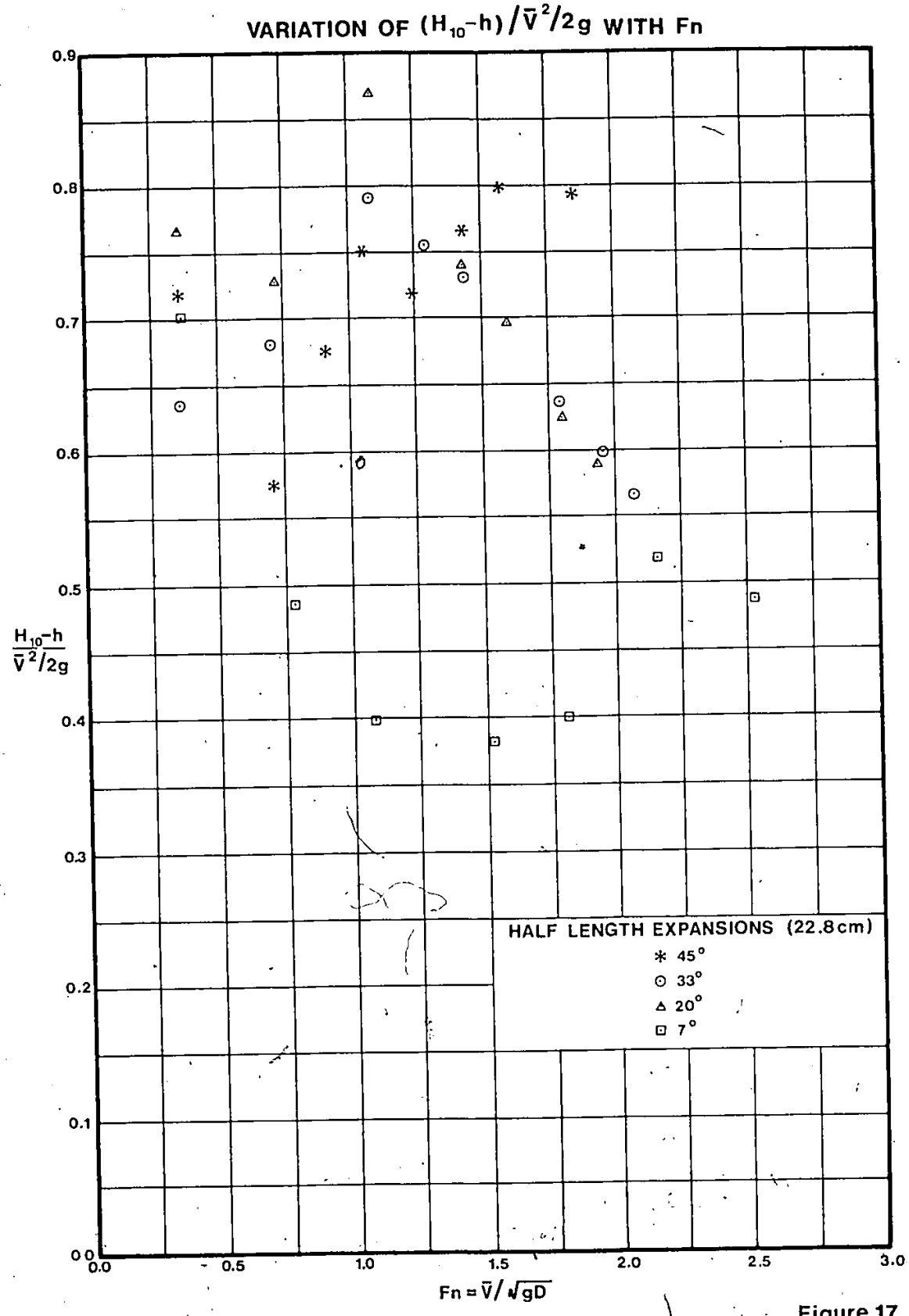
VARIATION OF $(H_{10}-h)/\bar{V}^2/2g$ WITH Fn
$\frac{H_{10}-h}{\bar{V}^2/2g}$
0.0
0.1
0.2
0.3
0.4
0.5
0.6
0.7
0.8
0.9
0.0
0.5
1.0
1.5
2.0
2.5
3.0
Fn = $\bar{V}/\sqrt{gD}$
HALF LENGTH EXPANSIONS (22.8cm)
* 45°
⊙ 33°
△ 20°
⊡ 7°

Figure 17

investigated.

Of major importance is the superior performance of the longer expansions (L/D = 5.84) and particularly the 20° and 33° expansions in diminishing the input energy by 40 to 70 per cent over a wide range of Froude numbers.

Energy dissipation in the 22.8 cm expansions is much less than for the 45.7 cm expansions. This is expected since the possibility for the jet to alter position is greater in wider or longer expansions, hence more turbulence. This shifting of jet position was evident from the position of the dome and the dye study described in Sec. 4.3. Rapid changes of jet position were evident for the 20° and 33° expansions; however, the 45° expansion, most likely due to its width, produced a fairly stable dome.

### 4.2.3 Dome Fluctuations

A possible drawback to the use of horizontal-crested, linear pipe expansions as service reservoir inlets is the rather severe fluctuations in both the height and the position of the dome. These fluctuations could cause lateral movement of the expansion. Such vibrations would place a strain on the pipe unless it were rigidly positioned. This inherent instability in dome position and the collapsing and subsequent redevelopment of the dome was most evident for the 20° and 33° expansions (the ones which displayed the lowest maximum dome heights).

An investigation of a method of reducing this movement was performed and is described in Sec. 4.4. The cause of this erratic movement of the dome was revealed in the dye study,

described in Sec. 4.3.

The dye study indicated that the jet did, in fact, break away from the walls of the expansion at, or very near, the entrance to the expansion. However, for all discharges, of a signifigant magnitude, in the 20° and 33° expansions, the jet would run upwards along the inside face and rarely straight up the center portion. The 45° expansion generally had the dome positioned in the center portion. If the dome shifted to the edge, it was returned to the center by swirling the water with a hand or just "shaping" the jet with a hand until it remained stable at the center. The freedom that the jet had in the 45° expansion is perhaps the reason for the way that the ratio of the maximum dome height to the kinetic energy changes with the Froude number.

It is evident from Figures 14 and 15 that this ratio for the 45° expansion is the lowest of all the expansions tested for low discharges and then gradually increases with increasing discharge until it is higher than the values for the other linear expansions tested, with the exception of the 45.7 cm, 7° expansion.

## 4.3 Dye Study

A dye study was performed to determine if the jet breaks away from the walls of the expansion at a point where the diameter is very little different than that of the approach pipe. If this was so, then the mean velocity in the approach pipe could be taken as the signifigant velocity in calculating

the theoretical rise of the water jet. The investigation did, in fact, determine that the jet does break away from one or both walls depending on the expansion angle and the rate of flow.

The findings are best discussed by observing the photographs taken using the half-section, 45.7 cm expansions with potassium permanganate dye injected into the pipe. The dye was added at a point about 2 meters (26 diameters) before the entrance to the expansions. The front plate of each of the expansions was made of plexiglass sheeting and the inside of each expansion was painted white.

Since the $7^{o}$ expansion is not much wider than the straight pipe, it was difficult to see the point of separation of the flow. The best photograph of this separation is shown as Plate 22. This shot was taken when the discharge was 0.34 l/s or 0.68 l/s for the full-section expansion. Adding to the difficulty of seeing the separation is the mixing that occurs at the edge of the jet. Photographs taken at higher discharges indicated similar flow separation; however, at some high discharges, such as 10.6 l/s (see Plate 8), the dome was clearly toward an edge indicating that the jet was probably adhering to the wall of the expansion and not rising up the center.

Low discharges in the $20^{o}$ expansion produced conflicting results. For most of the time, the jet would not rise vertically, but would break-away from one edge and cling to the other. This is evident in Plate 24, which shows the

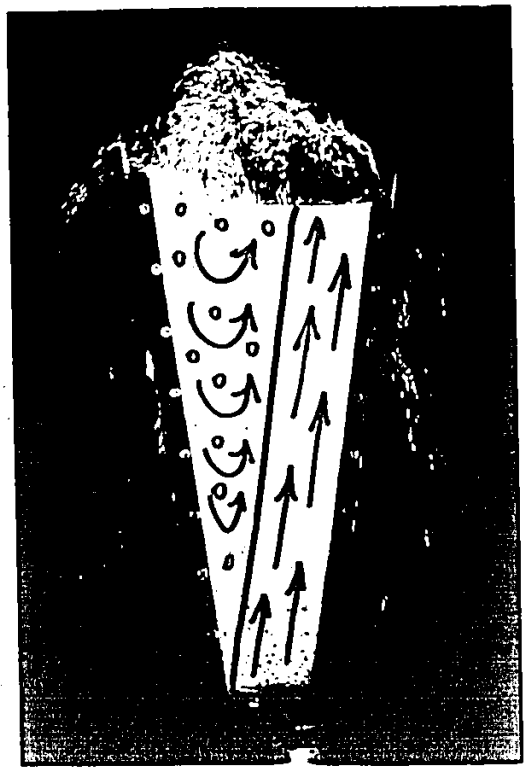

Plate 21. - $20^0$ Half-Section Expansion ($Q_e$ = 14.0 l/s)

This shot was taken from the left and slightly below. The discharge was 7.0 l/s which is equivalent to 14.0 l/s for the full-section expansion. The jet is running up the right edge. Air bubbles are being pulled down to the inlet.

Plate 22. - $7^0$ Half-Section Expansion ($Q_e^1$ = 0.68 l/s)

For such a small internal angle it is difficult to see the jet separation from the walls due to the slight amount of mixing that occurs.

[1] the discharge, $Q_e$, is the equivalent, full-section discharge.

Plate 23. - $20^0$ Half-Section Expansion ($Q_e$ = 3.82 l/s)

Separation is definitely occurring near the entrance to the expansion, but the jet is favouring the right side.

Plate 24. - $20^0$ Half-Section Expansion ($Q_e$ = 1.47 l/s)

The clear or white area is the jet. The jet goes up the right side and gradually moves away from the plexiglass plate toward the back of the expansion.

Plate 25. - $33^0$ Half-Section Expansion ($Q_e$ = 1.5 l/s)

As for the $20^0$ expansion, the jet would rise in the center for low discharges only. Plate 26 is the same expansion under greater discharge.

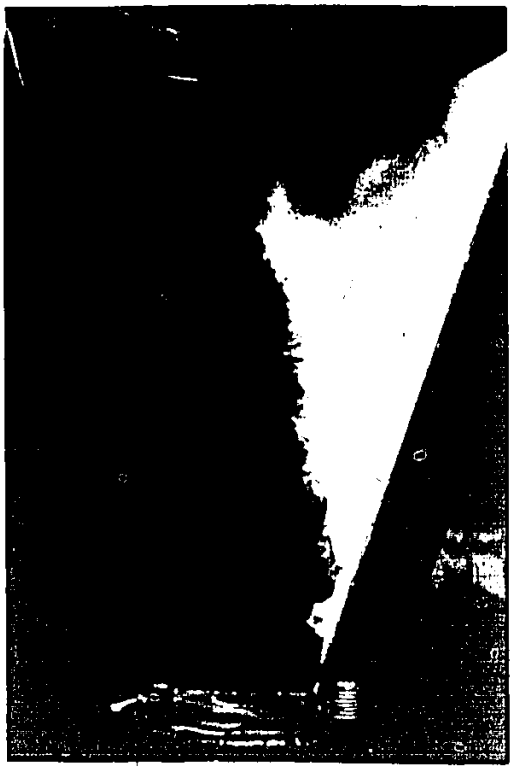

Plate 26. - $33^0$ Half-Section Expansion ($Q_e$ = 4.28 l/s)

Compare to Plate 25.

Plate 27. - $45^0$ Half-Section Expansion ($Q_e$ = 0.68 l/s)

Plate 28. - $45^0$ Half-Section Expansion ($Q_e$ = 2.83 l/s)

At discharges of approximately 4.25 l/s and higher, the jet would rise vertically or run up an edge.

20° expansion under a full-section discharge of 1.47 l/s. Plate 23 indicates that a more central rise can occur - the discharge was 3.82 l/s. Higher discharges always produced results similar to that shown in Plate 24. In this photograph, the jet moves to the right and then gradually back from the plexiglass plate. The jet would also cling to the other side.

Tests on the 33° expansion produced results similar to those obtained for the 20° expansion except that the jet would rise vertically more often and for higher discharges. For equivalent full-section discharges of less than 3.0 l/s, the jet was observed to rise only along the centerline, as in Plate 25. In the range of 3.0 to about 3.3 l/s, the jet position altered frequently between that shown in Plate 25 and that in Plate 26. Discharges above 3.3 l/s produced jet profiles similar to that shown in Plate 28.

For discharges up to approximately 4.4 l/s in the 45° expansion, the jet always rose vertically and flow separation occurred at the entrance to the expansion. Above 4.4 l/s the jet would sometimes run up the center and, at other times, up the wall. Plates 27 and 28 show the half-section, 45° expansion under equivalent full-section discharges of 0.69 l/s and 2.83 l/s respectively. This characteristic central tendency compliments the comments made in Sec. 4.2.3 about the stability of the dome for the 45°, full-length expansion.

In summary, it is clear that the jet does break away from the walls of the expansion at a point where the diameter is very little different than that of the approach pipe. However, there is a definite tendency for the jet to cling to the walls of the expansion.[1] This tendency is greater for small expansion angles and for larger discharges. This finding is reinforced by observations of the position of the dome recorded for each discharge and each expansion tested. This tendency for the jet to cling to the walls of the expansion was not easily visible for the 7° expansion due to the size constraint; however, an inspection of Plate 8, which shows the 7°, 45.7 cm expansion under a discharge of 10.6 l/s, verifies this.

4.4 Slotted Expansions

Section 4.2 pointed out the rather severe fluctuations in both the height and the position of the dome- most evident for the 20° and 33° expansions. There is nothing that can be done to prevent the collapsing and rebuilding of the dome which will occur, to some extent, even in the case of bellmouth expansions. The collapsing of the dome is not a design problem, however, rather this action assists in reducing the maximum dome height. The rapid shifting of the dome position is considered a problem, however, due to the strain that would be placed on the inlet pipe as a result of induced vibrations. This dome movement can be prevented by various methods.

---

1. due to pressure drop caused by high flow just inside inlet

One method that should reduce the shifting of the dome is to keep the jet off the wall of the expansion and to train it up the center. When the dome wandered during testing of the 45° expansion, a quick swirling motion with the hand in the expansion resulted in a shifting of the jet back to the central position. The swirling motion could be induced by a spiralling fin attached to the expansion walls. This method was not investigated but is recommended to the designer concerned about vibration.

The second approach is to ignore the path of the jet until a short distance below the crest. At this location a series of slots around the circumference will result in a lateral discharge which produces a much more centralized and stable dome. The degree of stabilization is related to the size of the slots in addition to the expansion angle and the discharge. Tests of this method of reducing the shifting of the dome were conducted on the 7°, 20°, 33° and 45°, 45.7 cm expansions. Three slots of equal length and equally spaced were cut in each of the expansions to provide a total opening of one-third of the circumference, 1.27 cm high and centered 4.45 cm below the crest of the expansions.

As expected, there was little change in the performance of the 7° expansion; since there was virtually no fluctuating of the maximum dome height position without the slotting. The 20° slotted expansion displayed a more central dome position than the non-slotted expansion and perhaps reduced the dome shifting, but not by an appreciable amount.

The results for the 33° expansion were rather good. Fluctuations in dome position were greatly reduced and the dome was much better centered. The 45°, slotted expansion produced a stable dome position. Plates 29 to 35 show the slotted expansions in operation.

The findings of the experimental investigation of the slotted expansions are presented in Figures 18 and 19. The dome height which was achieved for 10 per cent of the time was divided by the kinetic energy at the inlet of the expansion. This ratio was then plotted as a function of the Froude number (see Figure 18). The reduction in the range of the Froude number investigated (from that for the unslotted expansions) was a function of the reduction in discharge passing directly over the crest of the expansion (for the minimum Froude number) and the length of the Level-Tel probe (for the maximum Froude number).

To calculate the energy dissipation in the slotted expansions, the overflow water level was subtracted from the maximum dome height. Figure 19 was produced from the data presented in Figure 18 by subtracting the overflow water level, h, from the dome height which was reached or exceeded for 10 per cent of the time. The plot for the 7° expansion in Figure 18 is of little value, as was mentioned for the nonslotted, full-length expansion in Sec. 4.2. Due to the small angle of expansion, the dome has a signifigant influence on the discharge passing over the crest and through the slots; therefore, the effective overflow water level is less than

Plate 29. - $45^0$ Slotted Expansion (Q = 0.82 l/s).

Plate 30. - $45^0$ Slotted Expansion (Q = 10.7 l/s)

($F_n$ = 2.71) Dome is stable at center.

Plate 31. - $33^0$ Slotted Expansion (Q = 9.82 l.s)

The dome is more stable than for the non-slotted expansion. ($F_n$ = 2.49)

Plate 32. - $20^0$ Slotted Expansion (Q = 11.6 l/s)

See also Plate 33. ($F_n$ = 2.93)

Plate 33. - $20^0$ Slotted Expansion (Q = 11.6 l/s)

($F_n$ = 2.93)

Plate 34. - $20^0$ Slotted Expansion (Close-Up)

Notice the dome is on the right side.

$Q = 5.72$ l/s. $F_n = 1.45$

Plate 35. - $7^0$ Expansion (Slotted) (Q = 1.22 l.s)

The air "piping" running between the slots was evident for this expansion at low discharges. This reduced the water level a little.

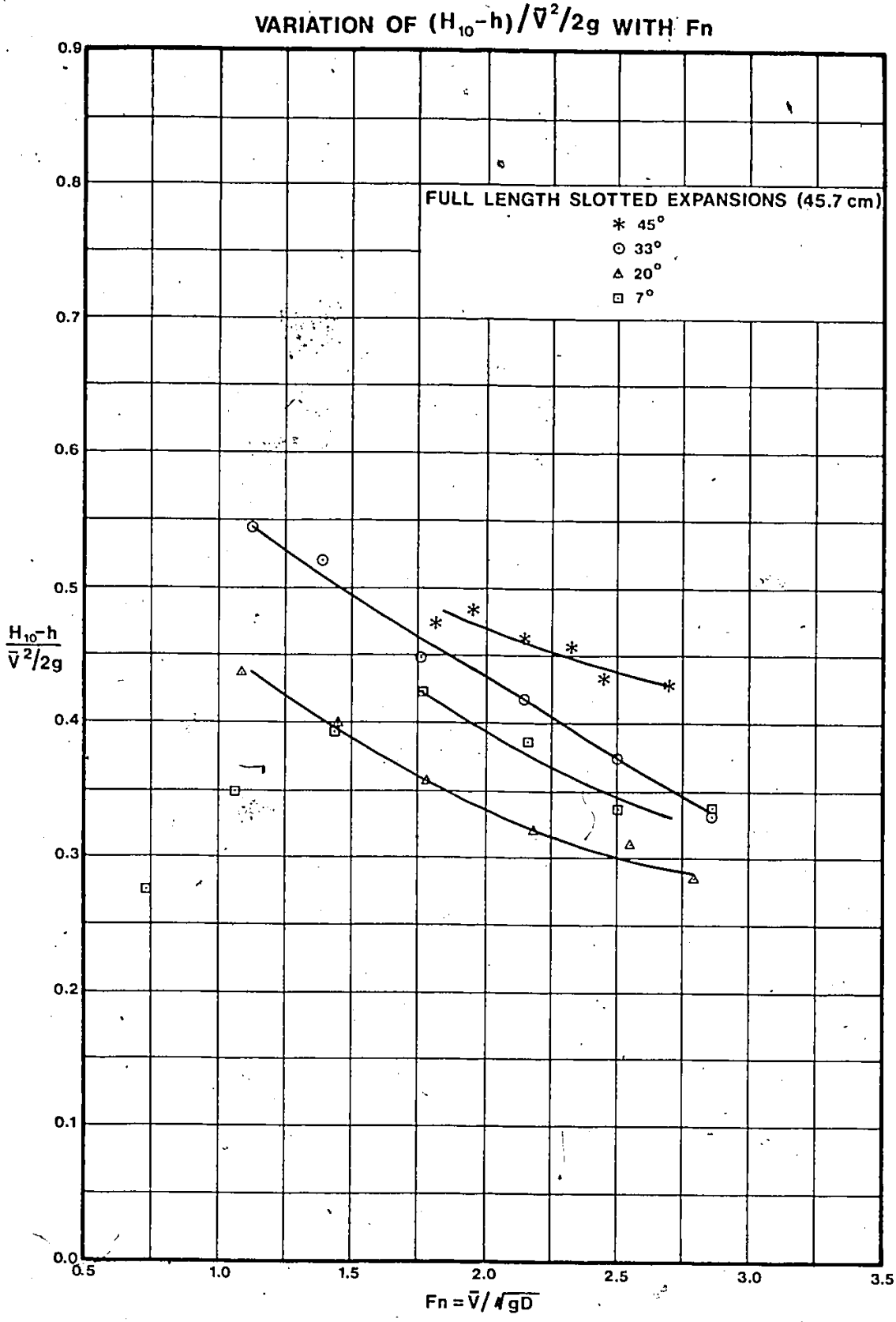
VARIATION OF $(H_{10}-h)/\bar{V}^2/2g$ WITH Fn
FULL LENGTH SLOTTED EXPANSIONS (45.7 cm)
* 45°
⊙ 33°
△ 20°
⊡ 7°
$\frac{H_{10}-h}{\bar{V}^2/2g}$
0.0
0.1
0.2
0.3
0.4
0.5
0.6
0.7
0.8
0.9
0.5
1.0
1.5
2.0
2.5
3.0
3.5
$Fn = \bar{V}/\sqrt{gD}$

Figure 18

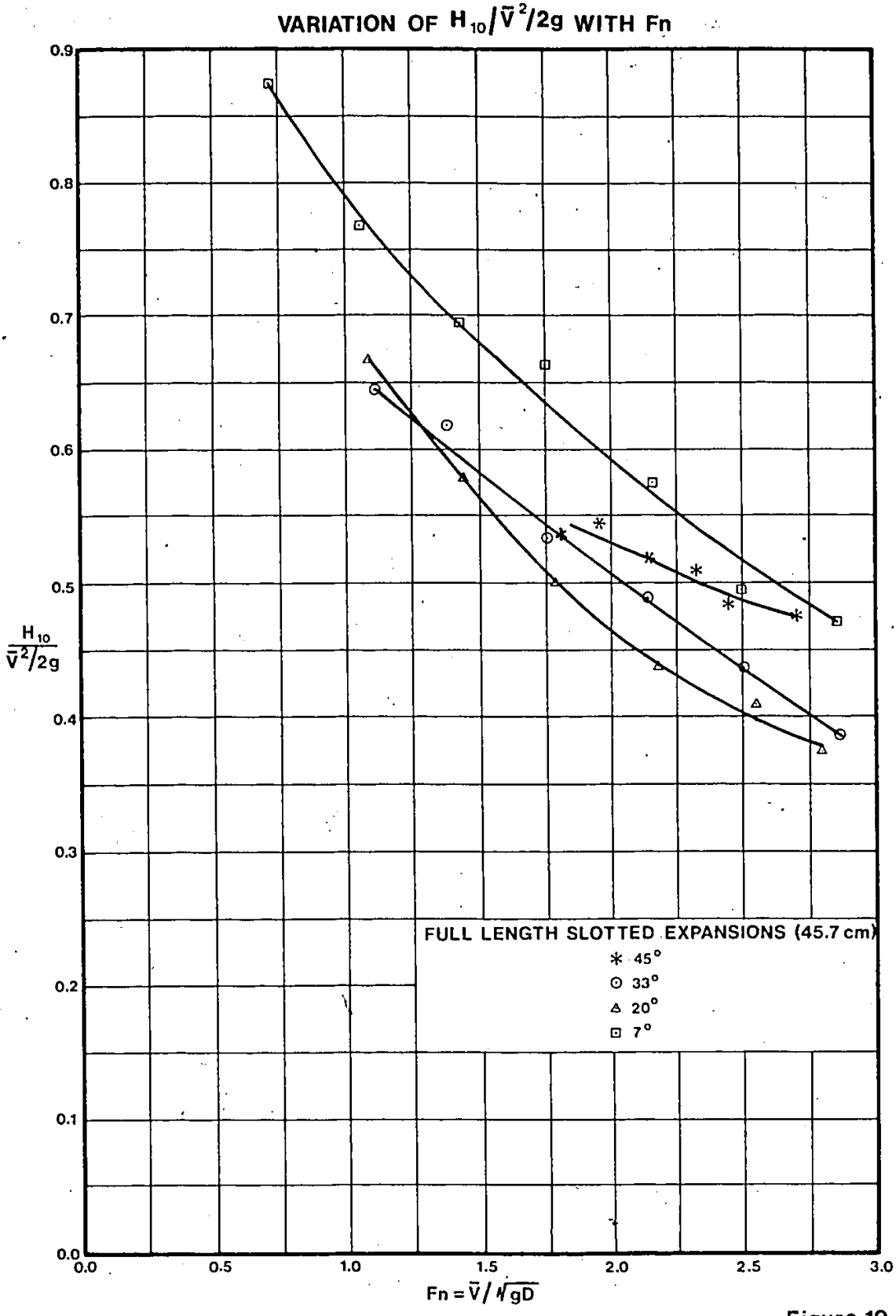
VARIATION OF $H_{10}/\bar{V}^2/2g$ WITH Fn
$\frac{H_{10}}{\bar{V}^2/2g}$
0.0
0.1
0.2
0.3
0.4
0.5
0.6
0.7
0.8
0.9
0.0
0.5
1.0
1.5
2.0
2.5
3.0
$Fn = \bar{V}/\sqrt{gD}$
FULL LENGTH SLOTTED EXPANSIONS (45.7 cm)
* 45°
⊙ 33°
△ 20°
⊡ 7°

Figure 19

that calculated in the normal way.

Disregarding the results for the 7° expansion, it is seen from Figures 14 and 19 that less energy is lost to turbulent mixing and or dome collapsing for the slotted expansions. This can be attributed to the reduction in fluctuation of the dome position. The 20° slotted expansion has a greater energy loss to turbulent mixing than the 33° expansion. This is the opposite to that for the non-slotted expansions (see Fig. 14), and is no doubt due mainly to the only slight reduction in dome fluctuations for the 20° expansion compared to the great reduction in fluctuation evidenced for the 33° expansion.

The overflow water level for the slotted expansions was determined by combining discharge relationships for the non-slotted expansion with discharge relationships developed for the slots. These relationships for the slots of the slotted expansions are shown in Figure 20. As can be seen in this Figure, a linear relationship develops, between the head of water over the crest of the slots raised to the power 1.5 and the discharge well before the water level reaches the crest of the expansion. The equations representing the linear portion of these discharge relationships for the slots are presented in Table 4.

These relationships for the slots were then added to those for the non-slotted expansions to produce the equations presented in Table 5. It was assumed that the discharge through the slots would continue to increase in

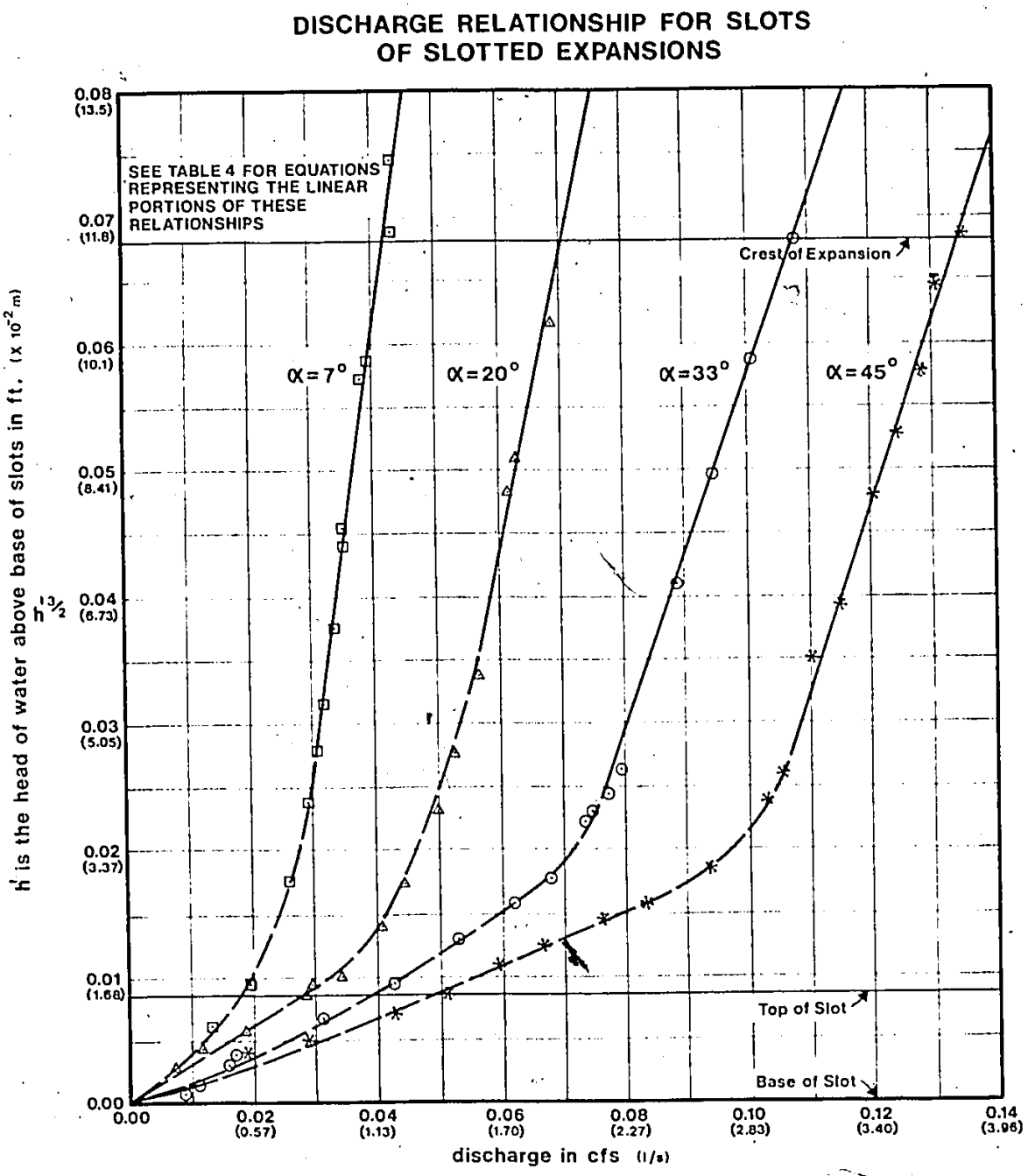
DISCHARGE RELATIONSHIP FOR SLOTS
OF SLOTTED EXPANSIONS
SEE TABLE 4 FOR EQUATIONS REPRESENTING THE LINEAR PORTIONS OF THESE RELATIONSHIPS
α=7°
α=20°
α=33°
α=45°
Crest of Expansion
Top of Slot
Base of Slot
h' is the head of water above base of slots in ft. (x 10⁻² m)
h^3/2
0.08 (13.5)
0.07 (11.8)
0.06 (10.1)
0.05 (8.41)
0.04 (6.73)
0.03 (5.05)
0.02 (3.37)
0.01 (1.68)
0.00
0.00
0.02 (0.57)
0.04 (1.13)
0.06 (1.70)
0.08 (2.27)
0.10 (2.83)
0.12 (3.40)
0.14 (3.96)
discharge in cfs (l/s)

Figure 20

Table 4. - Equations for Linear Portion of Discharge Relationships for Slotted Expansions (see Fig. 20).

| Slotted Expansion | Discharge Equation |
|---|---|
| $7^{o}$ | $Q_s = 48.9h'^{1.5} + 0.63$ |
| $20^{o}$ | $Q_s = 70.5h'^{1.5} + 1.18$ |
| $33^{o}$ | $Q_s = 120h'^{1.5} + 1.68$ |
| $45^{o}$ | $Q_s = 117h'^{1.5} + 2.48$ |

$Q_s$ is the discharge through the slots in l/s.

$h'$ is the head of water over the base of the slots in meters.

Table 5. - Equations to Determine the Overflow Water Level for the Slotted Expansions.

| Slotted Expansion | Discharge Equation |
|---|---|
| 7° | $Q = 48.9(h + 0.0508)^{1.5} + 1100h^{1.5} + 0.63$ |
| 20° | $Q = 70.5(h + 0.0508)^{1.5} + 1950h^{1.5} + 1.18$ |
| 33° | $Q = 120.(h + 0.0508)^{1.5} + 2880h^{1.5} + 1.68$ |
| 45° | $Q = 117.(h + 0.0508)^{1.5} + 4200h^{1.5} + 2.48$ |

Q is the discharge from the expansion in l/s.

h is the overflow water level above the crest of the expansion in meters.

accordance with the relationships in Table 4. It was further assumed that the overflow water level, h, increased by 0.0508 m (i.e. the distance from the crest to the base of the slots), was the appropriate head to apply in the equations for the discharge through the slots.

In summary to this discussion of the slotted expansions it should be mentioned that, although a reduction in the fluctuation of the dome is achieved, the storage capacity of the service reservoir would be reduced by the distance from the crest of the expansion to the base of the slots plus the increase in maximum dome height.

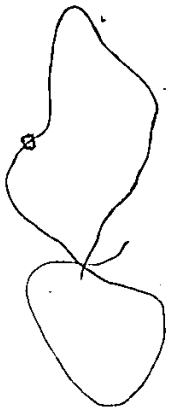

# CHAPTER 5

## CONCLUSIONS AND RECOMMENDATIONS

### 5.1 Conclusions

The following conclusions have been made as a result of this investigation:

1. Horizontal-crested linear expansions provide a signifigantly lower maximum dome height than the equivalent bellmouth expansion. Tests performed with the 33° expansion and the bellmouth indicate that this reduction varies from about 25 per cent at $F_n = 0.5$ to 40 per cent or more at $F_n = 3.0$. This reduction is due to the larger space in the linear expansion between the edge of the jet and the expansion walls compared to the bellmouth. In the linear expansion, energy is dissipated by the inducement of turbulent mixing in this space.

This being the case, the maximum recommended elevation of the crest, for linear expansions, would be greater than that for the equivalent bellmouth unit; hence, the equivalent linear expansion provides a corresponding increase in reservoir storage capacity.

2. Longer expansions provide a greater reduction in maximum dome height. For a given discharge, the 33° expansions provided a reduction of 50 per cent or more in the maximum dome height by doubling the length from 22.8 cm to 45.7 cm ($L/D = 2.92$ to $L/D = 5.84$). A slight reduc-

tion of 10 to 20 per cent was obtained for the 7° expansion, while the 20° and 45° expansions had reductions of about 40 per cent.

This reduction of the maximum dome height with increased length of the expansion is due to the greater space available for turbulent mixing.

3. Maximum dome heights[1] were determined over a wide range of discharge ($F_n$ = 0.4 to 2.9)[2] for 10 inlet structures. These were the 7°, 20°, 33° and 45°, 22.8 cm linear expansions and the 7°, 20°, 33° and 45°, 45.7 cm linear expansions; and the bellmouth and straight pipe extension.

Of these expansions, the lowest maximum dome height was achieved for the 33°, 45.7 cm linear expansion for which L/D was 5.84. The ratio of the maximum dome height to the kinetic energy of the flow at the inlet to the expansion drops from near 1.0 at $F_n$ = 0.6 to 0.5 at $F_n$ = 1.3 and to 0.3 at $F_n$ = 2.9. It would appear that this ratio will not fall below 0.25 for values of $F_n$ much greater than 3.0.

4. The bellmouth, straight pipe extension and

---

[1] the maximum dome height is the level to which the water rises or exceeds for 10 per cent of the time.

[2] The Froude number, $F_n$ is defined in this thesis to be:

$$F_n = \frac{\bar{V}}{\sqrt{gD}}$$

the 7° expansions had domes which did not shift position, even for very high discharges. Of the 20°, 33° and 45° linear expansions, the 45°, 45.7 cm expansion displayed the most stable and central dome position. The 20°, 22.8 cm linear expansion (L/D = 2.92), on the other hand, had a very rapidly shifting dome.

This rapid altering of the dome position for the 20° and 33° expansions could cause a severe strain in the inlet pipe unless the pipe and, or, the expansion were rigidly positioned.

5. The addition of horizontal slots, located just below the crest of the expansion produces a much more central and stable dome. This was observed for the 45.7 cm linear expansions with three slots of equal length, providing a total opening of 33 per cent of the circumference, 1.27 cm high and centered 4.45 cm below the crest of the expansion.

The greatest improvement was noticed for the 33° expansion. The dome for the 45° expansion never moved from the center, whereas, for the non-slotted expansion, some shifting had occurred.

As expected, less energy is lost in the 20° and 33° slotted expansions than in the non-slotted expansions. This is the result of decreased dome collapsing and turbulent mixing in the slotted expansions. The 20° slotted expansion, due to the smaller amount of slot opening and, hence, less reduction of dome fluctua-

tions, produces a smaller maximum dome height, for a given discharge.

6. For all of the expansions investigated, the overflow water level, h, necessary to pass the flow, passing through the expansion, over the expansion crest has been subtracted from the maximum dome height, $H_{10}$. The values of $H_{10} - h$ were expressed as a ratio of the kinetic energy of the flow at the inlet to the expansion and were plotted as a function of the Froude number.

These data points represent the portion of the kinetic energy which has been converted to potential energy. The remaining energy has been lost due to mixing induced by the jet and to the interference between the rising and falling water in the dome.

7. To transfer the results of this investigation from the model (laboratory) scale into the performance of a prototype expansion several factors must be considered. These are:

a) The data presented in Figures 16 and 17 (ratios of $H_{10} - h$ to the kinetic energy of the flow at the inlet to the expansion) must be used.

b) Knowledge of the height of water over the crest of the prototype as a function of discharge is required to determine the maximum dome height, $H_{10}$.

c) The prototype must be geometrically similar to the model and the Froude numbers identical. Thus the following scaling relations must hold;

$$n_{\alpha} = 1$$

$$n_L = n_D$$

$$n_Q = n_D^{2.5}$$

8. When the necessary scale adjustments are made to make Sellin's (1) experimental results on the expansions shown in Figure 5 compatible to the larger diameter expansions investigated in this study, the agreement is quite good. To compare Sellin's results, take the ratios of $H_{10}/ V^2/2g$ and $(H_{10} - h)/ V^2/2g$ shown in Figures 6 and 7 and divide these ratios by 1.5 (since this is the ratio of the diameters, $n_D$). The numbers obtained in this manner can be compared to the results of this study by ensuring that the scale of $F_n$ in Figures 6 and 7 is contracted by taking the square root of this value.

The use of the Level-Tel probe should have resulted in less error than the approximate method which Sellin used.

## 5.2 Recommendations for Further Research

The following studies are recommended as extensions to the present work:

1. Testing should be undertaken in a prototype situation to determine the validity of the scaling rules presented in this and Sellin's (1) work.

2. Another laboratory investigation could be undertaken to explore the performance of linear expansions with internal angles in the range of $20^{\circ}$ to $45^{\circ}$. The object of this study would be to determine if an angle other than $33^{\circ}$ will provide a smaller maximum dome height.

3. Several more expansion lengths could be investigated to determine the change in maximum dome height with L/D over a greater range.

4. Tests should be conducted to determine the effects of the dome fluctuations on the inlet piping. If adequate bracing is provided, then this study is not necessary.

5. Testing of the spiral ribbing technique as a method of reducing the fluctuation in the dome position while still reducing the maximum dome height is recommended.

REFERENCES

1. Sellin, R.H.J., Horizontal-Crested Bellmouths as Service Reservoir Inlets, Journal of the Institution of Water Eng. - Britain, Vol. 20, No. 8, November, 1966, pp.518-522.
2. Cederwall, K., Gross Parameter Solutions of Jets and Plumes, Journal of the Hydraulics Division, ASCE, Vol. 101, No. HY5, May, 1975, pp. 489-509.
3. Fan, L.N., and Brooks, N.H., Numerical Solution of Turbulent Buoyant Jet Problems, Report No. KH-R-18, W.M. Keck Laboratory, California Institute of Technology, Pasadena, Calif., 1969. (Reference made in 2.)
4. List, E.J., and Imberger, J., Turbulent Entrainment in Buoyant Jets and Plumes, Journal of the Hydraulics Division, ASCE, Vol. 99, No. HY9, Proc. Paper 9992, Sept., 1973, pp. 1461-1474.
5. Albertson, M.L., et al., Diffusion of Submerged Jets, Transactions, ASCE, Vol. 115, Paper 2409, 1950, pp 639-664.